CZECH TECHNICAL UNIVERSITY IN PRAGUE

FACULTY OF MECHANICAL ENGINEERING

Department of Process Engineering

CFD Simulation of Heat Transfer in an Agitated Vessel

Master thesis

Arunanshu Chakravarty

Name of the supervisor: Ing. Karel Petera, Ph.D.

2017

FACULTY OF MECHANICAL ENGINEERING CTU IN PRAGUE

MASTER THESIS ASSIGNMENT

I. PERSONAL AND STUDY INFORMATION

Surname:	**Chakravarty**	First name:	**Arunanshu**	Personal no.:	**452958**
Faculty:	**Faculty of Mechanical Engineering**				
	Department of Process Engineering				
Study program:	**Mechanical Engineering**				
Study field:	**Process Engineering**				

II. MASTER THESIS SPECIFICATION

Master thesis title (in Czech):

Master thesis title (in English):

CFD simulation of heat transfer in an agitated vessel

Elaboration guidelines:

- Make a literature research concerning the heat transfer in agitated vessels.
- Create a flow and heat transfer model of an agitated vessel with pitched-blade turbine impeller in ANSYS CFD.
- Perform numerical simulations of heat transfer in the agitated vessel for different rotation speeds and compare the simulation results with experimental data.
- Summarize the methodology used in the thesis and propose possible improvements of the solution procedure..

Literature resources:

Name and affiliation of the thesis supervisor:

Ing. Karel Petera Ph.D., Department of Process Engineering FME CTU in Prague

Consultant:

-

Assignment issue date: **10th April 2017** Thesis due date: **6th June 2017**

Validity of assignment: -

Thesis Supervisor	Head of the Department	Dean of the Faculty

III. THESIS ASSIGNMENT RECEIVED

The student is aware that the thesis has to be accomplished through an independent and unassisted student's work, supported only by recognized consultations. Literature and other information resources as well as consultants' names have to be acknowledged in the thesis.

26-04-2017	
Date	Student

Declaration

I hereby declare that I have completed this thesis entitled **CFD Simulation of Heat Transfer in an Agitated Vessel** independently with consultations with my supervisor and I have attached a full list of used references and citations.

I do not have a compelling reason against the use of the thesis within the meaning of Section 60 of the Act No.121/2000 Coll., on copyright, rights related to copyright and amending some laws (Copyright Act).

In ...Prague..., Date: ..... ……

ACKNOWLEDGEMENT

I would like to express my sincere gratitude and respect towards my thesis supervisor, Dr. Karel Petera. The fruitful discussions with him were of great help for the successful completion of the work and I learned a lot from him.

I would like to express my love and affection towards my parents to whom I owe so much that can never be repaid and to my younger brother for his moral support and encouragement throughout my career. I would like to thank my friend, MUDr. Joana Forte for always motivating me and her proof reading of this text.

ABSTRACT

The present work was carried out to numerically investigate the flow field and transient heat transfer in a cylindrical agitated vessel mounted with a pitched blade turbine (PBT) impeller in the turbulent flow regime. The sliding mesh technique available in ANSYS Fluent was used to model the flow around the impeller and $k-\omega$ based Shear-Stress-Transport (SST) turbulence model was chosen to model turbulence. The grid independency study was performed to find the acceptable grid size that provides a solution with good accuracy. The power characteristics of the PBT impeller were determined and the obtained non-dimensional Power numbers were compared with the experimental work. The unsteady heat transfer during heating of a batch of liquid was evalutated by performing transient simulations and the obtained Nusselt numbers were compared with the calculated values based on heat balance. The heat transfer correlations were developed and compared with the experimental work.

Keywords: agitated vessel, pitched blade turbine, sliding mesh, CFD, transient heat transfer

CONTENTS

Chapters	Title	Page No.
	LIST OF FIGURES	viii
	LIST OT TABLES	ix
	NOTATIONS	x
Chapter-I	**Introduction and Objectives of this work**	
1.1	Introduction	1
1.2	Objectives of this work	2
Chapter-II	**Theory of Agitated Vessels**	
2.1	Introduction	3
2.2	Agitated Vessel Construction	3
2.3	Types of Agitated Vessel	6
2.4	Estimation of Heat Transfer in Agitated Vessels	7
Chapter-III	**Heat Transfer in Agitated Vessels**	
3.1	Dimensionless Groups	8
	3.1.1 Reynolds number	8
	3.1.2 Prandtl number	8
	3.1.3 Nusselt number	9
3.2	Heat Transfer Correlations for Agitated Fluids	9
3.3	Estimation of Time for Heating	10
3.4	Estimation of Mixing Time	11
Chapter-IV	**Computational Fluid Dynamics**	
4.1	Introduction	13
4.2	Governing Equations for Viscous Flows	13
	4.2.1 The Continuity Equation	14
	4.2.2 The Momentum Equation	14
	4.2.3 The Energy Equation	15
4.3	Solution of Governing Equations	16
4.4	Turbulence Moedeling	17
4.5	$k-\omega$ SST Turbulence model	18
4.6	CFD approach to Problem Solution	19
Chapter-V	**Numerical Method and Model Description**	
5.1	Introduction	20
5.2	Geometrical Parameters of Agitated Vessel	20
5.3	Geometrical Model of Agitated Vessel	21
5.4	Computational Grid	21

Chapters	Title	Page No.
5.5	Mesh Quality	21
5.6	Modeling the Flow around Impeller	22
	5.6.1 Moving Reference Frame	22
	5.6.2 Sliding Mesh Technique	22
Chapter-VI	**Numerical Analysis of Flow Field in Agitated Vessel**	
6.1	Introduction	24
6.2	Numerical Computation of Flow Field	24
6.3	Solution Procedure	25
	6.3.1 Material	26
	6.3.2 Solver	26
	6.3.3 Cell Zone Conditions	27
	6.3.4 Boundary Conditions	27
	6.3.5 Solution Method	27
6.4	Computational Results	28
	6.4.1 The velocity field	28
	6.4.2 Checking y^+ at the tank surfaces	29
Chapter-VII	**Examination of Spatial (Grid) Convergence**	
7.1	Introduction	31
7.2	Method – Grid Convergence Index	31
7.3	Evaluation of Grid Convergence Index	31
7.4	Calculation of Grid Convergence Index	34
Chapter-VIII	**Power Characteristics of Impeller**	
8.1	Introduction	37
8.2	Dimensionless Group – Power number	37
8.3	Calculation of Power number for 6 Blade PBT Impeller	38
Chapter-IX	**Transient Heat Transfer in Agitated Vessel**	
9.1	Introduction	42
9.2	Transient (or unsteady) Heat Transfer	42
9.3	Heat Transfer Surfaces	43
9.4	Numerical Analysis of Heat Transfer	43
9.5	Solution Procedure	44
9.6	Computational Results	44
	9.6.1 Correction of ANSYS Fluent heat transfer coefficients	44
	9.6.2 Calculation of Nusselt number	46
	9.6.3 Heat Transfer Correlation	47
	Concusion and Further Scope	51
	References	53

LIST OF FIGURES

Figure No.	Description	Page No.
2.1	Conventional cylindrical agitated vessel with top entering impeller	3
2.2	Standard vessel configuration	4
2.3	A four blade Pitched Blade Turbine (PBT)	5
4.1	$k-\omega$ SST Turbulence model blends $k-\omega$ and $k-\varepsilon$ model	18
5.1	Geometrical parameters of cylindrical vessel	20
5.2	Geometrical model and computational grid of agitated vessel	21
5.3	Sliding mesh orientations in 2-D	23
6.1	Axial flow pattern generated by the PBT impeller discharging the flow downwards towards the vessel bottom	28
6.2	Velocity contour plot for Re = 36860	28
6.3	Axial velocity profile in the discharge flow of the PBT impeller	29
6.4	y^+ range for the tank bottom at $n = 500$ rpm	30
6.5	y^+ range for the tank wall at $n = 500$ rpm	30
6.6	y^+ range for the tank baffles at $n = 500$ rpm	30
7.1	Non-monotonic dependency of the monitored quantity	36
8.1	Obtained power characteristic of 6 blade PBT impeller in turbulent flow regime	38
8.2	Functional relationship between Power number Po and Reynolds number Re described by power model and null hypothesis	41

LIST OF FIGURES

Figure No.	Description	Page No.
9.1	Effect of varying agitation rate on the heat transfer coefficient	46
9.2	Obtained data and fitted correlations compared with the experimental work of Chapman et al. (1964)	50

LIST OF TABLES

Table No.	Description	Page No.
3.1	Heat Transfer Correlation for Jacketed vessel with different impellers	10
5.1	Mesh quality measures for the generated grid	22
6.1	Run-time for simulations based on mixing time	24
7.1	Calculation of discretization error	35
8.1	Calculation of Power number	38
9.1	Obtained heat transfer coefficients	45
9.2	Obtained Nusselt numbers	46
9.3	Calculated Nu for different Re	48

NOTATIONS

Parameters of Agitated Vessel

B	baffle width [m]
C	clearance between impeller and vessel bottom [m]
H	liquid height [m]
T	diameter of vessel [m]
t_m	mixing time [s]
Z	vessel height [m]

Parameters of Impeller

D	impeller diameter [m]
R	impeller radius [m]
n	impeller rotation speed [rpm]
t	blade thickness [m]
θ	pitch angle of blade [deg]
u_{tip}	tip velocity of impeller blade [m s^{-1}]
ω_i	angular velocity of impeller [rad s^{-1}]
S_{bl}	blade width [m]
P	power input of impeller [W]

Fluid properties

ρ	density of fluid [kg m^{-3}]
μ	dynamic viscosity of fluid [Pa.s]
μ_b	dynamic viscosity for the bulk of fluid [Pa.s]
μ_w	dynamic viscosity of fluid at wall [Pa.s]
c_p	specific heat capacity of fluid [J kg^{-1} K^{-1}]
λ_f	thermal conductivity of fluid [W m^{-1} K^{-1}]

Flow velocities

$\vec{u}$	instantaneous velocity [m s^{-1}]
$\bar{u}$	mean flow velocity [m s^{-1}]
u_i	velocity components in the x-, y- ,z- direction [m s^{-1}]

Dimensionless numbers

Re	Reynolds number [-]
Pr	Prandtl number [-]
Nu	Nusselt number [-]
nt_m	dimensionless rotational speed [-]
Po	Power number [-]

Turbulence modeling

k	turbulent kinetic energy [$m^2\ s^{-2}$]
ε	kinetic energy dissipation rate [$m^2\ s^{-3}$]
ω	specific dissipation [s^{-1}]

Heat transfer analysis

A	heat transfer area [m^2]
G_c	geometry correction [-]
h	heat transfer coefficient [$W\ m^{-2}\ K^{-1}$]
T	temperature [K]
T_h	temperature of the heating medium [K]
T_b	temperature of the batch liquid [K]
T_{init}	initial temperature [K]
T_{ref}	reference temperature [K]
T_w	wall temperature [K]
$\Delta\bar{T}_{ln}$	logarithmic mean temperature difference [K]
m	batch liquid mass [kg]
q	heat flux [$W\ m^{-2}$]
U	overall heat transfer coefficient [$W\ m^{-2}\ K^{-1}$]
Vi	viscosity ratio [-]

Chapter I Introduction and Objectives of this Work

1.1 Introduction

So far, an extensive amount of research has been focused on studying the phenomenon of mixing which is commonly encountered in process engineering applications in the chemical, pharmaceutical, petrochemical, fermentation, bio-reactor, food industries etc. The term mixing implies homogenizing single or multiple phases in terms of concentration of components. Agitation is one of the mechanisms of mixing that is often utilized in process applications for homogenizing the temperature and physical properties of components. The key equipment for mixing process is the mixer equipped with some sort of arrangement to ensure an efficient mixing process. An agitated vessel is one of the types of process equipment employed for the mixing and homogenizing batch of process fluid.

In a mechanically stirred vessel, agitation is usually accomplished by a centrally mounted impeller which rotates in contact with the process fluid (to be homogenized) in a cylindrical vessel which may or may not be equipped with baffles. The baffles provide a favorable circulation of batch during the mixing process by breaking the undesirable vortexes. The impeller type and number of blades is chosen in such a way so as to provide an efficient mixing process.

In process engineering applications, it is often required to heat or cool the batch during the mixing process. This simultaneous mixing with heat transfer is accomplished by the use of either a jacketed vessel mounted externally to the vessel or a heat transfer coil placed inside the vessel. An arrangement with an external heat exchanger circuit is also possible. The main parameter to be evaluated in heat transfer analysis of agitated vessels is the process side heat transfer coefficient which depends on a number of factors including the impeller speed, its type, vessel geometry, the regime of flow inside vessel, etc.

Generally, the design of agitated vessels is based on the determination of various design parameters by experimental results obtained on the laboratory scale models. These results are then scaled-up and utilized in the fabrication of actual vessels used in industrial applications. This empirical approach is without a doubt an excellent way to obtain the design parameters with the only drawback being the high investment and the experimental time and labor. Due to the advent of digital age and high speed computing it is now possible to make a preliminary design and analysis before the initial experimental stage to obtain the design parameters and to observe the different possible design scenarios without huge investments on experimental set-ups. This is mainly attributed to the numerical analysis field of computational fluid dynamics, commonly abbreviated as CFD, using computational power to solve the numerical analysis problem of fluid flows and heat transfer.

1.2 Objectives of this work

The present work was carried out to fulfill the following primary objectives:

a) To solve the flow field inside the agitated vessel equipped with baffles in the whole domain by numerical computational approach.

b) To utilize CFD sliding mesh technique in conducting the transient analysis of heat transfer in a jacketed cylindrical agitated baffled vessel mounted with a 45^{o} PBT (pitched blade turbine) impeller for different rotation speeds.

c) To compare the obtained results with the available literature and to propose further scope related to the present work.

Chapter II Theory of Agitated Vessels

2.1 Introduction

The agitated vessels are process equipments utilized to realize the industrial mixing process. The following section provides a brief overview about agitated vessels and their types.

2.2 Agitated Vessel Construction

A majority of the process engineering applications utilize cylindrical agitated vessel equipped with baffles to realize the mixing process. A typical mechanically stirred agitated vessel with its parts is shown in Figure 2.1.

A standard agitated vessel used as reference for comparing different designs is shown in Figure 2.2.

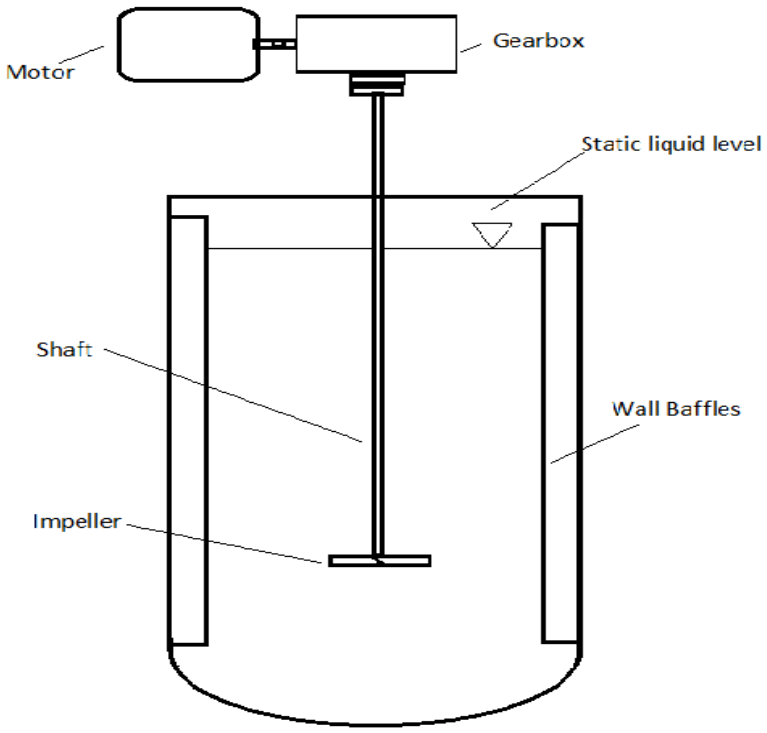

Fig. 2.1: Conventional cylindrical agitated vessel with top entering impeller

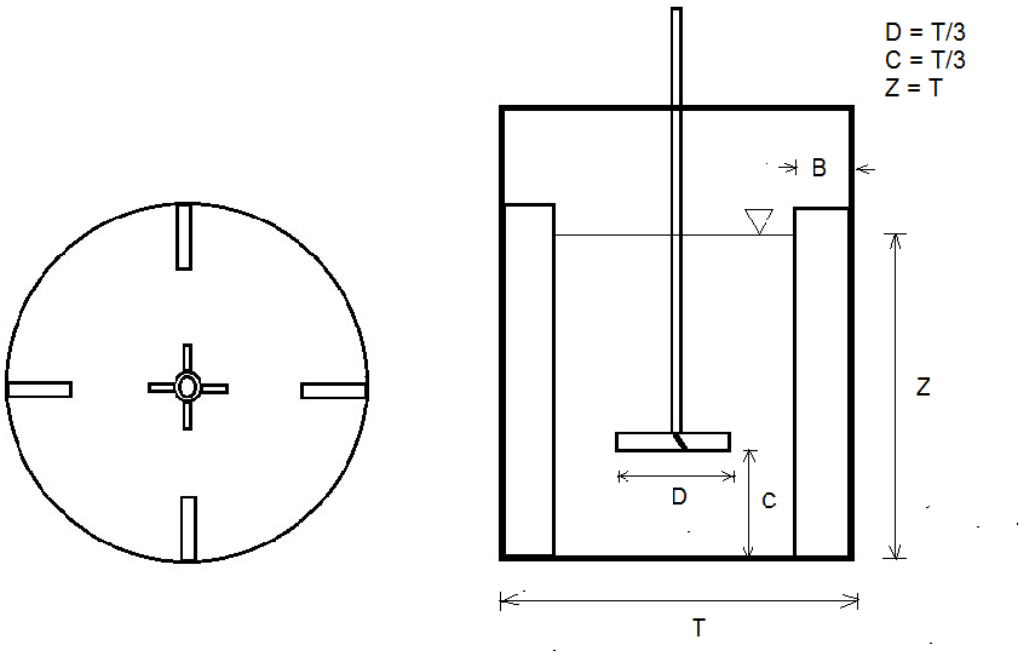

Fig. 2.2: Standard vessel configuration

In Standard vessel configuration, the impeller diameter, D is 1/3 of the vessel diameter, T. The impeller height, C from the tank bottom is also 1/3 of the vessel diameter. The liquid level, Z is equal to the vessel diameter. The four baffles have width, B of 1/10 of vessel diameter (Chisholm, 1988).

The main components of an agitated vessel are:

1. Impeller
2. Shaft
3. Gearbox
4. Motor
5. Wall Baffles

Impeller : Impeller is the key rotating component of the agitated vessel. The mixing performance and the energetic requirements are strongly affected by the proper choice of impeller for the particular application.

Impeller Types: The impellers are broadly classified based on flow pattern such as axial flow impellers and radial flow impellers. Axial flow impellers discharge the process fluid with the axial flow velocity component and are mainly used for blending, solids suspension and heat transfer applications. A special type of axial flow impeller is the PBT (pitched blade turbine)

on which the blades have a pitch angle ranging from of 10^{o}-90^{o} are bolted and tack-welded on the impeller hub in such a way that the flow pattern consists of both the axial and radial flow velocity components. Hence pitched blade turbine is considered a mixed flow impeller. In this work PBT type impeller was chosen with a pitch angle of 45^{o}. A typical PBT impeller is shown in Figure 2.3.

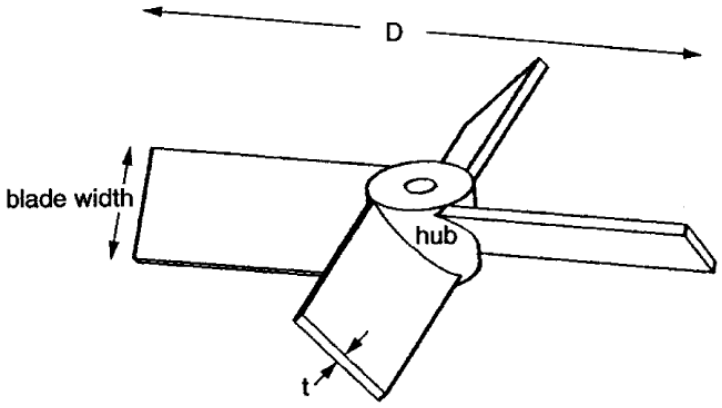

Fig. 2.3: A four blade Pitched Blade Turbine (PBT), (Chapple, et al., 2002)

Radial flow impellers discharge process fluid radially outward towards the vessel wall and are commonly used for low to medium viscosity fluids.

Shaft : The impellers are mounted on the shaft with proper shaft sealing. The shafts must be designed to bear the loading encountered during service conditions.

Motor/Gearbox : It consist of the drive to the agitator. The proper selection criteria depends on the pumping capacity and power requirements of the agitated vessel.

Wall Baffles : Wall baffles are rectangular surfaces positioned in the way of tangential flows of process fluid generated by a rotating impeller. It has a significant effect on mixing performance. In the absence of baffles, the flow generated by impeller rotation is two dimensional and causes swirling action. Wall baffles eliminate this swirling motion by transforming these tangential flows to the vertical flows providing top-to-bottom mixing. The baffles are usually radially mounted to ensure a favorable circulation of batch during mixing process by breaking the undesirable vortexes.

2.3 Types of Agitated Vessel

A conventional agitated vessel is generally a vertical cylindrical stirred tank. Vessels with rectangular or square cross-sections are also used for specific applications. The vessel bottom can be flat, dished or ellipsoidal type. The main criteria that specify particular agitated process equipment is its key component which in the case of agitated vessels is an impeller. The agitated vessels are distinguished on the basis of different arrangements and the type of impeller mounted on it. The classification of agitated vessels is categorized:

On the basis of flow pattern in the vessel:

a) vessel with axial impellers
b) vessel with radial impellers

On the basis of position of agitator in the vessel:

a) vessel with top-entering centrally mounted impeller
b) vessel with bottom-entering agitator
c) vessel with side-entering mixer
d) vessel with angular top-entering mixer

On the basis of heat transfer surfaces

a) vessel with surrounding jacket
b) vessel with an internal heat transfer coil
c) vessel with external heat exchanger circuit

The heat transfer in agitated vessel is described in more detail in the subsequent sections. Selection criteria for a particular vessel type depend on the application for which it will be used. For example a typical requirement in industrial mixing is the blending of components to acquire uniform concentration. Such a vessel does not require any heat transfer and therefore agitated vessels without heat transfer surfaces can be selected. Another application area involves the mixing of process fluid with the intention of heating/cooling the process fluid at the same time where mixing enhances heat transfer in general. In such applications, it is necessary to equip vessels with proper heat transfer surfaces. Additional requirements are the proper selection of vessel agitators, their positions, the agitator power requirements and the available floor area.

2.4 Estimation of Heat Transfer in Agitated Vessels:

When the process application in agitated vessel requires heat addition or removal from the process fluid, the vessel is equipped with suitable heat transfer surfaces. The fluid motion generated by the agitator enhances the heat transfer coefficient. The most commonly used heat transfer surfaces are jackets, internal helical coils, and internal baffle coils. A jacket can be, in a simplified way, a vessel outside the main vessel with an annular space for the flow of service fluid, baffled, half-pipe, or dimpled. Heat transfer fluid is supplied on the service side of the heat transfer surfaces.

The calculation of heat transfer in an agitated vessel is commonly based on some form of Dittus-Boelter equation which is used to calculate the process side heat transfer coefficient. The equation is of the form:

$$Nu = C\ Re^{a}\ Pr^{b} Vi^{c} \tag{2.1}$$

where, Nu is Nusselt number, Re is Reynolds number, Pr is Prandtl number and Vi is the wall viscosity correction factor. The exponents a, b and c are empirically determined along with the system coefficient (C). For Jacketed vessels, the typical values for a, b and c are 0.67, 0.33 and 0.14 respectively with system coefficient ranging from 0.33 to 1 depending on the impeller type , the Reynolds number, installed baffling, type of vessel bottom head, clearances and number of impeller blades.

After obtaining the exponents of Eq. (2.1), the process side heat transfer coefficient (h) can be determined and the overall heat transfer coefficient (U) can be evaluated which is finally used to estimate the time of heating or cooling a particular batch from an initial known temperature. The theory of heat transfer in agitated vessels is described in the following chapter.

Chapter III Heat Transfer in Agitated Vessels

3.1 Dimensionless Groups

The analysis of the heat transfer in agitated vessels is greatly simplified by the dimensionless groups. The dimensional analysis is a convenient tool to reduce the number of independent variables. The heat transfer correlations are presented in terms of these dimensionless groups. Some of the commonly used dimensionless groups encountered in the heat transfer analysis of agitated vessels are described in the following section.

3.1.1 Reynolds number

In characterizing the regime of flow in an agitated tank, Reynolds number (Re) is evaluated. It is described by the following equation:

$$Re = \frac{nd^2\rho}{\mu} \tag{3.1}$$

where d is the impeller diameter, n is the rotational speed of impeller in rev/s, ρ is density of process fluid and μ is dynamic viscosity of process fluid. Based on the Reynolds number the flow in stirred tanks is usually considered laminar for Re < 50, transitional for 50 <Re<5000 and fully turbulent for Re > 5000. However, the transition also depends on the Power number (Po) of the impeller which is a function of Reynolds number for laminar flows and approaches a constant value in turbulent flows. Power number is described in Chapter VIII.

3.1.2 Prandtl number

Another dimensionless group that is utilized in the heat transfer analysis of agitated vessels is Prandtl number (Pr) described by the relation:

$$Pr = \frac{\mu_b c_p}{\lambda_f} \tag{3.2}$$

where μ_b is the dynamic viscosity for the bulk of fluid, c_p is specific heat of fluid and λ_f refers to the thermal conductivity of fluid.

3.1.3 Nusselt number

For evaluating heat transfer to or from the vessel wall (or bottom) in a jacketed vessel the Nusselt number (Nu) is used which is described by the relation:

$$Nu = \frac{h\,D}{\lambda_f} \tag{3.3}$$

where h is process side heat transfer coefficient, D is vessel diameter and λ_f is thermal conductivity of fluid. The evaluation of Nusselt number permits the calculation of heat transfer coefficient and ultimately the heating/cooling time for a particular batch of fluid from an initial known temperature.

3.2 Heat Transfer Correlations for Agitated Fluids

The heat transfer correlations enable the process engineer to predict the amount of transferred heat with reasonable accuracy. Heat transfer correlations for agitated fluids are obtained by conducting experiments on a scaled-down version of plant equipment. This requires the fulfillment of geometrical, kinematic and dynamic similarities between the scaled model tank and the plant equipment. There are many correlations depending on the type of vessel, i.e. jacketed or helical coil, depending on impeller type, their sizes, relative locations within the vessel, presence of baffles, etc. However all of the correlations can be converted in the general form as:

$$Nu = C\ Re^{a}\ Pr^{b} Vi^{c}\ G_c \tag{3.4}$$

where

$$Vi = \frac{\mu_b}{\mu_w} \tag{3.5}$$

is the Sieder-Tate correction for temperature-dependent dynamic viscosity, μ_w of fluid at wall and dynamic viscosity, μ_b of fluid at the bulk of flow. G_c in Eq. (3.4) is geometric correction factor.

Typical values of the constant and exponents for jacketed vessel equipped with different type of impellers is shown in Table 3.1 reproduced from the book, Chisholm, 1988.

Table 3.1: Heat Transfer Correlation for Jacketed vessel with different impellers

Impeller	**N_b**	**Baffles**	C	**Exponents of**		
				Re	Pr	Vi
Paddle	2	Yes	0.415	2/3[a]	1/3	0.24
		No	0.112	3/4	0.44	0.25
Various turbines: disk, flat, and pitched blade	6	No	0.54	2/3	1/3	0.14
Propeller		Yes	0.74	2/3	1/3	0.14
	3	No	0.37	2/3	1/3	0.14
		Yes	0.5	2/3	1/3	0.14

a : Relatively low range of Reynolds numbers, 20-4000. The other correlations presented in this table were developed for ranges of *Re* reaching 10^5 and more.

3.3 Estimation of Time for Heating

The heat transfer correlations discussed in the previous section enable the process engineer to estimate the overall heat transfer coefficient U that provides the information about the amount of heat to be transferred. In practical applications, it is also necessary to determine the time required to heat or cool a particular batch of liquid in an agitated vessel.

The time estimate for heating a batch of liquid in a jacketed vessel with constant temperature heating medium is obtained as:

The heat transfer rate can be calculated from the equation:

$$Q = m\, c_p \frac{dT_b}{dt} = UA(T_h - T_b) \tag{3.6}$$

where T_h is the temperature of the heating medium, e.g. steam, T_b is the temperature of the batch liquid, m is batch liquid mass, c_p is the specific heat capacity of the batch liquid.
Eq. (3.6) can be rearranged as:

$$\frac{dT_b}{T_h - T_b} = \frac{U\,A}{m\,c_p}\,dt \tag{3.7}$$

and integrated over the time interval Δt required to heat the agitated liquid batch from temperature T_{b1} to T_{b2} :

$$\int_{T_{b1}}^{T_{b2}} \frac{dT}{T_h - T_b} = \frac{U\,A}{m\,c_p} \int_0^{\Delta t} dt \tag{3.8}$$

which results into :

$$ln\left(\frac{T_h - T_{b1}}{T_h - T_{b2}}\right) = \frac{U\,A}{m\,c_p}\,\Delta t \tag{3.9}$$

From Eq. (3.9) the heating time Δt, can be calculated.

3.4 Estimation of Mixing Time

In an agitated vessel containing a batch of liquid to be mixed, the time required to achieve a certain degree of homogeneity starting from a completely segregated state is referred to as the mixing time, t_m. It is a useful parameter to assess the mixing efficiency of the process. It can be determined experimentally by injecting a tracer and following its concentration at a fixed point in the tank and subsequently determining the concentration response. The mixing time is reached when the concentration of tracer becomes relatively steady and the fluid composition approaches uniformity.

The mixing time, t_m depends on different variables such as size of the tank, impeller size and type, fluid properties such as its viscosity and impeller rotational speed. A criteria used for characterizing the mixing time is dimensionless rotational speed of the impeller defined by nt_m, where n is the impeller rotational speed in rev/s.

In general, the dependency of mixing time on other quantities may be expressed as:

$$nt_m = f\left(\frac{nd^2\rho}{\mu}\right) = f\,(Re) \tag{3.10}$$

For low value of Reynolds number, the dimensionless rotational speed, nt_m, is a function of Reynolds number and for high values of Reynolds number, nt_m reaches a constant value. The critical values are experimentally determined for different impeller types. The nt_m represents the number of stirrer rotations required to homogenize the fluid.

In the present work, the mixing time was evaluated for different Reynolds numbers corresponding to rotational speeds ranging between 100 – 900 rpm. The simulation run-time was based on the theoretically evaluated mixing time, t_m. The heat transfer coefficients were determined based upon reaching this time, t_m in the agitated vessel. The heating time for reaching a particular temperature can be determined from Eq. (3.9) by substituting the evaluated heat transfer coefficients determined for time, t_m and hence the heat transfer coefficients can be evaluated corresponding to the heating time.

Chapter IV Computational Fluid Dynamics

"The purpose of computing is insight, not numbers"
- R.W Hamming

4.1 Introduction

The use of computers to solve the fluid flow and heat transfer related problems is referred to as computational fluid dynamics or in abbreviated form as CFD. The accuracy of results of numerical solution of transport phenomenon problem by CFD analysis is often debated in comparison to the experimentally obtained results. However, if the solution approach of CFD analysis is such that it is based on accurate problem set-up and computational procedure, then the results can be treated with reasonable accuracy comparable to the experimentally obtained values. But again, this strongly depends on the CFD user's knowledge in defining the problem and performing simulations. The advantages of choosing CFD analysis over experimental study are:

a) CFD analysis is often inexpensive
b) Parametric studies with different variables can be done with ease
c) The problem can be simplified by assumptions

The essence of computational fluid dynamics lies in the numerical solution of governing equations of fluid flow and heat transfer phenomenon. The following sections describe in detail these governing equations and the CFD approach to their solutions.

4.2 Governing Equations for Viscous flows

The governing equations are mathematical statements that describe the physics of the fluid flow and are based on three fundamental physical principles of conservation of mass, Newton's second law of motion and conservation of energy. The basis of CFD is numerical solution of three fundamental governing equations of continuity, momentum and energy.

These governing equations in *conservation form* for unsteady, three-dimensional, compressible, viscous flows are discussed in subsequent sections

4.2.1 The Continuity Equation

Continuity equation in conservation form obtained by applying the principle of conservation of mass on a control volume *fixed in space* and described in differential form is:

$$\frac{\partial \rho}{\partial t} + \nabla.(\rho\vec{u}) = 0 \tag{4.1}$$

where $\vec{u}$ is the flow velocity at a point on the control surface, $\vec{u} = f(x, y, z, t)$ and ρ is the density of fluid. For incompressible flows, Eq. (4.1) is simplified to

$$\nabla.\vec{u} = 0 \tag{4.2}$$

4.2.2 The Momentum Equation

The conservation form of momentum equation by the application of Newton's second law of motion to a fixed fluid element is described by three scalar equations corresponding to x, y and z directions and for viscous flows they are termed as Navier – Stokes equation.
The conservation form is described as:

$$\rho\left[\frac{\partial \vec{u}}{\partial t} + (\vec{u}.\nabla)\vec{u}\right] = -\nabla p + \nabla.\vec{\vec{\tau}} + \rho\vec{f} \tag{4.3}$$

where $\nabla.\vec{\vec{\tau}}$ is the viscous stress tensor and $\vec{f}$ is the body force per unit mass. The viscous stress tensor $\nabla.\vec{\vec{\tau}}$ for Newtonian fluids is given by (in tensor notation):

$$\tau_{ij} = \mu\left(\frac{\partial u_i}{\partial x_j} + \frac{\partial u_j}{\partial x_i} - \frac{2}{3}(\nabla.\vec{u})\delta_{ij}\right) \tag{4.4}$$

where δ_{ij} is the Kronecker-Delta operator which is equal to 1 if $i = j$, otherwise equals to zero, x_i denote mutually perpendicular coordinate directions and μ is the dynamic viscosity.

The Navier-Stokes equation in terms of three scalar components can be described as:

x-component of the momentum equation:

$$\frac{\partial(\rho u_x)}{\partial t} + \nabla.(\rho u_x \vec{u}) = -\frac{\partial \mathrm{p}}{\partial \mathrm{x}} + \frac{\partial \tau_{\mathrm{xx}}}{\partial \mathrm{x}} + \frac{\partial \tau_{\mathrm{yx}}}{\partial \mathrm{y}} + \frac{\partial \tau_{\mathrm{zx}}}{\partial \mathrm{z}} + \rho \mathrm{f_x} \qquad (4.5)$$

y-component of the momentum equation:

$$\frac{\partial(\rho u_y)}{\partial t} + \nabla.(\rho u_y \vec{u}) = -\frac{\partial \mathrm{p}}{\partial \mathrm{y}} + \frac{\partial \tau_{\mathrm{xy}}}{\partial \mathrm{x}} + \frac{\partial \tau_{\mathrm{yy}}}{\partial \mathrm{y}} + \frac{\partial \tau_{\mathrm{zy}}}{\partial \mathrm{z}} + \rho \mathrm{f_y} \qquad (4.6)$$

z-component of the momentum equation:

$$\frac{\partial(\rho u_z)}{\partial t} + \nabla.(\rho u_z \vec{u}) = -\frac{\partial \mathrm{p}}{\partial \mathrm{z}} + \frac{\partial \tau_{\mathrm{xz}}}{\partial \mathrm{x}} + \frac{\partial \tau_{\mathrm{yz}}}{\partial \mathrm{y}} + \frac{\partial \tau_{\mathrm{zz}}}{\partial \mathrm{z}} + \rho \mathrm{f_z} \qquad (4.7)$$

The equations (4.5, 4.6 and 4.7) are the Navier-Stokes equations in *conservation form*.
For incompressible flows the second term of the viscous stress tensor given in Eq. (4.4) is zero due to the incompressibility constraint given in Eq. (4.2). For constant viscosity, the Navier-Stokes equation for incompressible flows can be written as:

$$\rho\left[\frac{\partial \vec{u}}{\partial t} + (\vec{u}.\nabla)\vec{u}\right] = -\nabla \mathrm{p} + \mu\nabla^2\vec{u} + \rho\vec{\mathrm{f}} \qquad (4.8)$$

4.2.3 The Energy Equation

Energy equation is a mathematical statement representing the conservation of energy principle and for incompressible flows can be written as:

$$\rho c_p\left[\frac{\partial T}{\partial t} + \vec{u}.\nabla T\right] = \lambda\nabla^2 T + \vec{\vec{\tau}} : \vec{\vec{\Delta}} + \dot{\mathrm{q}}^{(\mathrm{g})} \qquad (4.9)$$

where c_p is specific heat at constant pressure, T is absolute temperature, $\vec{\vec{\tau}}$ is dynamic stress tensor, $\vec{\vec{\Delta}}$ is symmetric part of the velocity gradient tensor and $\dot{\mathrm{q}}^{(\mathrm{g})}$ represents internal heat sources or sinks. Eq. (4.9) is called Fourier-Kirchoff equation.

In addition to the previously mentioned governing equations of fluid dynamics, the additional equations also arise if the problem include diffusion phenomenon. However, in the present work the study was limited to homogeneous, non-reacting fluids.

4.3 Solution of Governing Equations

In the CFD analysis, the three set of equations described in the previous section, i.e. equation of continuity, momentum equation and energy equation are generally referred to as the full Navier-Stokes equation. The analytical solution to the complete Navier-Stokes equation for three dimensional fluid flows is not obtained yet by the scientific community. Therefore, the solution is based on numerical approach by using suitable discretization schemes that enables the transformation of partial differential equations (i.e governing equations) to the solvable algebraic equations. This is the basis of numerical modeling utilized in CFD analysis.

A common discretization scheme utilized in CFD analysis is the *Finite Volume Method*, which is based on dividing the computational domain into control volumes. The differential equations are integrated over the control volumes and divergence theorem is applied. To evaluate the derivatives, the values at the control volume faces are required, which is based on some assumption about its variation. The result is a set of algebraic equations one for each control volume which is solved iteratively. In the present work, ANSYS Fluent software package was used for CFD analysis which is based on Finite Volume Method.

An important consideration in the solution of incompressible flows is that the gradient of pressure term which appears in all the three momentum equations. But there is no explicit pressure equation available as there is no pressure term in the continuity equation. Therefore a Pressure-Velocity coupling algorithm is used to derive equations for the pressure from the momentum equations and continuity equation. In the present work, SIMPLE (Semi-Implicit Method for Pressure-Linked Equations) algorithm was selected for Pressure-Velocity coupling in ANSYS Fluent software.

4.4 Turbulence Modeling

In fluid flow, turbulence is characterized by random fluctuations of transported quantities such as flow velocity, pressure, temperature etc.

The instantaneous flow velocity, $\vec{u}$ can be described as:

$$\vec{u} = \bar{u} + u' \tag{4.10}$$

where $\bar{u}$ is the mean velocity and u' is the fluctuating component at that instant. In the Navier-Stokes equation which governs the velocity and pressure of fluid flow, the time-dependent velocity fluctuations are separated from the mean flow velocity by the averaging of the Navier-Stokes equation and the resulting equation obtained is called Reynolds-averaged Navier-Stokes (RANS) equations which govern the mean flow. However, velocity fluctuations are still present after the averaging in the form of a non-linear component which is termed as *Reynolds stress* which is a function of velocity fluctuations.

After the averaging of Navier-Stokes equation, the RANS equation can be written (in tensor notation), (White, F.M., 1974):

$$\rho\left(\frac{\partial \bar{u}_i}{\partial t} + \bar{u}_k \frac{\partial \bar{u}_i}{\partial x_k}\right) = -\frac{\partial \bar{p}}{\partial x_i} + \frac{\partial}{\partial x_j}\left(\mu \frac{\partial \bar{u}_i}{\partial x_j}\right) + \frac{\partial R_{ij}}{\partial x_j} \tag{4.11}$$

where R_{ij} is the Reynolds stress tensor,

$$R_{ij} = -\rho\overline{u'_\iota u'_\jmath} \tag{4.12}$$

To obtain closed form of equations that contain only the mean velocity and pressure, the Reynolds stress is modeled by *turbulence models* which employs Boussinesq hypothesis by introducing the concept of eddy turbulent viscosity.

$$R_{ij} = -\rho\overline{u'_\iota u'_\jmath} = \mu_t\left(\frac{\partial \bar{u}_i}{\partial x_j} + \frac{\partial \bar{u}_j}{\partial x_i}\right) - \frac{2}{3}\mu_t \frac{\partial \bar{u}_k}{\partial x_k}\delta_{ij} - \frac{2}{3}\rho k \delta_{ij} \tag{4.13}$$

where μ_t is turbulent viscosity,

$$\mu_t = \rho C_\mu \frac{k^2}{\varepsilon} \tag{4.14}$$

In Eq. (4.14), k represents the turbulent kinetic energy, ε represents kinetic energy dissipation rate and C_μ is an empirical constant. The calculation of turbulent viscosity

requires determination of turbulent kinetic energy and energy dissipation rate. The result of turbulence modeling is additional transport equations for k and ε which need to be solved. There are several turbulence models utilized in the CFD analysis like Spalart-Allmaras model, $k-\varepsilon$ model, $k-\omega$ model, etc. In the $k-\omega$ model, k represents the turbulent kinetic energy and ω represents specific dissipation rate. In the present work, $k-\omega$ SST turbulence model was chosen to model the turbulence in the agitated vessel.

4.5 $k-\omega$ SST Turbulence model

The $k-\omega$ based Shear-Stress-Transport (SST) turbulence model is designed to account for the transport of the turbulent shear stress and provides highly accurate predictions of the onset and the amount of flow separation under adverse pressure gradients by including the transport effects into the formulation of the eddy-viscosity. The $k-\omega$ SST model combines the $k-\omega$ model near the wall and $k-\varepsilon$ model in the free stream.

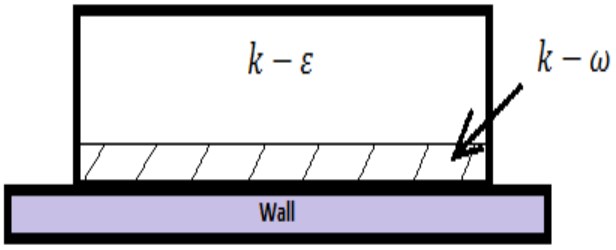

Fig. 4.1: $k-\omega$ SST Turbulence model blends $k-\omega$ and $k-\varepsilon$ model

The transport equations for $k-\omega$ SST model are (Fluent 6.3, User's Guide, 2006):

$$\frac{\partial(\rho k)}{\partial t}+\frac{\partial}{\partial x_i}(\rho k u_i)=\frac{\partial}{\partial x_j}\left(\Gamma_k\frac{\partial k}{\partial x_j}\right)+\tilde{G}_k-Y_k+S_k \tag{4.15}$$

and

$$\frac{\partial(\rho\omega)}{\partial t}+\frac{\partial}{\partial x_i}(\rho\omega u_i)=\frac{\partial}{\partial x_j}\left(\Gamma_\omega\frac{\partial \omega}{\partial x_j}\right)+G_\omega-Y_\omega+D_w+S_\omega \tag{4.16}$$

where $\tilde{G}_k$ represents generation of turbulent kinetic energy due to mean velocity gradients, G_ω represents generation of ω, Γ_k and Γ_ω represent effective diffusivity of ω, Y_k and Y_ω represent dissipation of k and ω due to turbulence, D_w represents cross-diffusion term, S_k and S_ω are the user-defined source terms.

4.6 CFD approach to Problem Solution

In CFD analysis, the fluid flow phenomenon is simulated by breaking down the fluid domain into discrete cells (called mesh) and the solver module of CFD solves RANS equation with conservation laws in each cell. The result is in the form of plots and contours of flow variables. The accuracy of CFD analysis depends on a number of factors such as the user's knowledge in defining the problem with proper selection of initial and boundary conditions, accuracy in modeling geometries, the generated mesh resolution and its quality; In general, the higher the number of mesh elements generated the better is the accuracy but it demands more computational power.

The next chapter describes the geometrical model and the computational grid that was utilized to solve the flow field inside the agitated vessel equipped with baffles.

Chapter V Numerical Method and Model Description

5.1 Introduction

In CFD analysis, the prerequisite for performing simulations is a modeled geometry defining the fluid domain with appropriate boundaries. The geometry is a scaled model of the actual vessel used in plant equipment. The geometrical parameters of the model are selected satisfying the geometrical similarity principles with the actual vessel. The following section describes the geometrical parameters of the agitated vessel used for CFD analysis in this work.

5.2 Geometrical Parameters of Agitated Vessel

The simulations were performed on a flat-bottom cylindrical agitated vessel with four equally spaced baffles mounted with a six blade PBT impeller. The impeller diameter, D is 0.066 m and blade angle 45^o. The impeller to vessel diameter ratio is $^D/_T = 0.33$. The impeller height above bottom, C is 0.040 m with $C/D = 0.66$ and $C/T = 0.2$. The vessel height, Z is equal to the vessel diameter, $T = 0.2$ m. The baffle width, B is 0.02 m and the baffles have zero clearance to the wall.

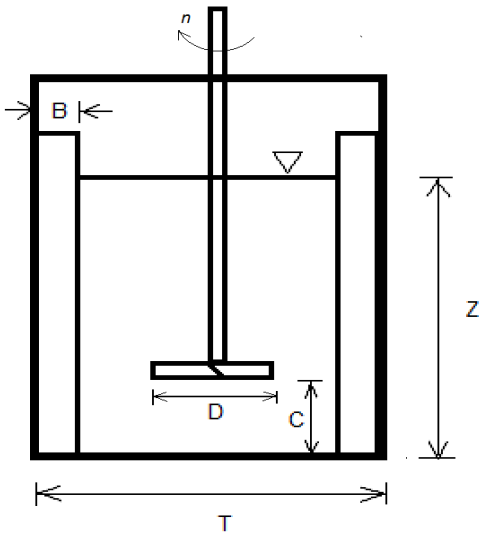

Fig. 5.1: Geometrical parameters of cylindrical vessel

5.3 Geometrical Model of Agitated Vessel

The present work is based on the model of the agitated vessel designed in the ANSYS Design Modeler. Figure 5.2 (a) shows the vessel geometry (in isometric view) consisting of a cylindrical tank with the impeller region and the equally spaced baffles.

5.4 Computational Grid

The modeled geometry was discretized using tetrahedral and hexahedral mesh elements in ANSYS Meshing. Tetrahedral mesh was generated near the impeller region and rest of the domain was discretized using Hexahedral meshing. The total number of mesh elements generated was 2,167,821 (more than 2 million). The computational grid generated is shown in Figure 5.2 (b).

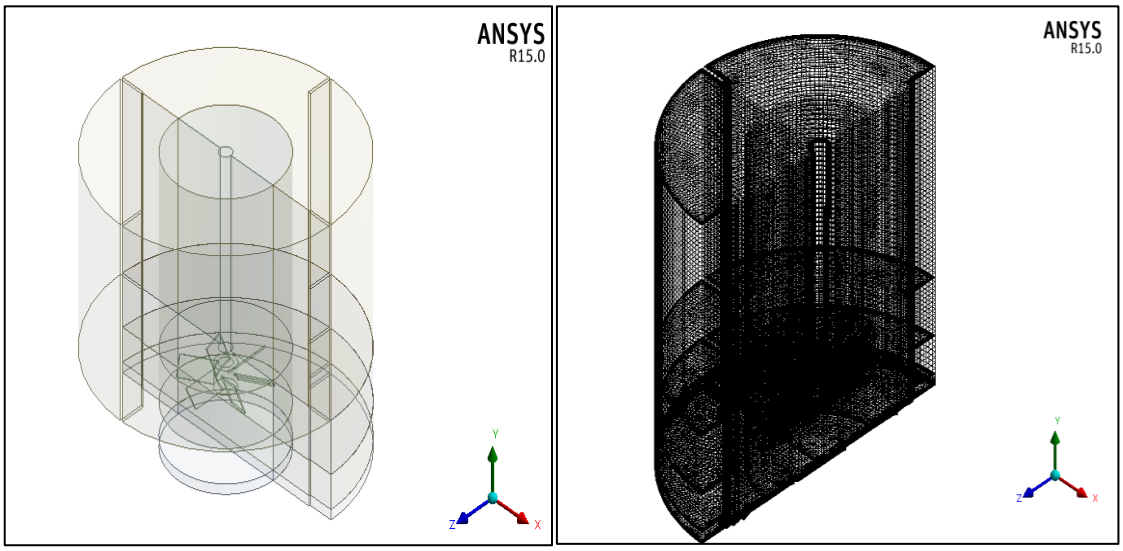

(a) **(b)**

Fig. 5.2: Geometrical model and computational grid of agitated vessel.

5.5 Mesh Quality

The accuracy of the result in CFD analysis depends on the quality of the generated mesh. The quality is judged by parameters like skewness, orthogonal quality, aspect ratio, etc. The obtained values of these mesh quality measures for the generated computational grid of agitated vessel are tabulated in Table 5.1.

Table 5.1: Mesh quality measures for the generated grid

Quality Measure	Value
Maximum Skewness	0.98
Minimum Orthogonal Quality	3.72736e-02
Maximum Aspect Ratio	3.0191e+02

The mesh quality measures (skewness, orthogonal quality) obtained and shown in Table 5.1 were not very satisfying. Therefore, we applied polyhedral conversion of highly skewed tetrahedral elements in the region around the impeller. This conversion improved the mesh quality substantially and it was confirmed by rechecking the mesh quality in ANSYS Fluent. After the conversion, the minimum orthogonal quality reported was 0.105521 and the maximum aspect ratio was 4.1447e+02.

5.6 Modeling the Flow around Impeller

Due to the rotation of the impeller in the agitated vessel, there is a presence of rotor-stator interaction between the impeller and surrounding non-wall boundaries (e.g. baffles). To take into account the effect of this rotor-stator interaction, there are different modeling techniques available for solution.These techniques are described in following sub-sections:

5.6.1 Moving Reference Frame

One way to model the rotor-stator interaction is the MRF (Moving Reference Frame) approach. The MRF technique is a simple, robust and efficient steady-state technique of CFD modeling. The MRF approach assumes an assigned volume (e.g. region between impeller blades) has a constant rotational speed and the non-wall boundaries are surfaces of revolution (e.g. cylindrical, spherical). In ANSYS Fluent, a separate fluid region containing the impeller is defined and for this region a Moving Reference Frame with a given rotational speed is specified. One flow field is calculated for one impeller position. MRF approach is used in problems where the interaction between rotor-stator is usually weak.

5.6.2 Sliding Mesh Technique

The present work was carried out to compute the unsteady flow field inside the baffled cylindrical agitated vessel. Therefore, to take into account the presence of baffles and their

interaction with the rotating impeller, another technique suitable for transient problems known as *Sliding Mesh* approach was used for modeling the time-accurate solution.

The Sliding Mesh technique is based on transient rotor-stator interactions in which the two or more cell zones are used and they are bounded by interface zones. The interface zones of the adjacent cell zones are associated with one another to form a mesh interface. The two cell zones move relative to each other along the mesh interface. In the course of calculation, the cell zones slide (i.e. rotate or translate) relative to one another along the mesh interface in finite steps. As the geometry of the impeller changes during calculation (due to its movement with respect to stationary geometry components), the mesh also changes.

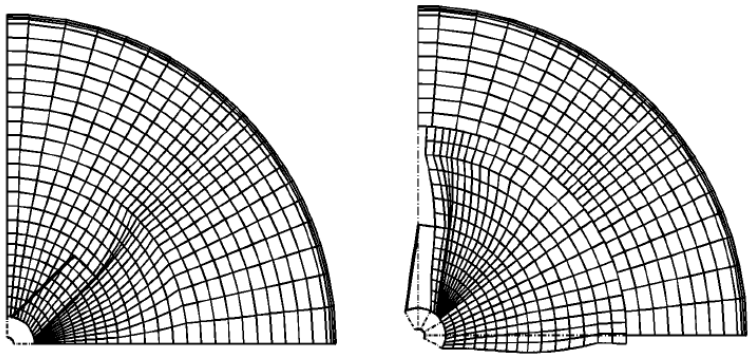

(a) (b)

Fig. 5.3: Sliding mesh orientations in 2-D (a) initial position (b) moved position, (Marshall, E.M and Bakker, A, 2004)

The Sliding Mesh technique is similar to the MRF approach as in both modeling techniques, a separate fluid region for the impeller is defined with the exception that in Sliding Mesh technique, the impeller region mesh should be disconnected from the mesh of the vessel region. The disconnection of impeller region mesh from the mesh of the vessel region was achieved by creating a separate part in the ANSYS Design Modeler and consequently, a non-conformal mesh interface was created in ANSYS Meshing.

Moreover the Sliding Mesh technique is more computing expensive than the MRF approach, mainly because it represents a transient simulation. The next chapter describes the solution procedure for the transient simulations performed for the modeled geometry of the agitated vessel to analyze the flow field and heat transfer.

Chapter VI Numerical Analysis of Flow Field in Agitated Vessel

6.1 Introduction

One of the objectives of this work is to investigate the flow field inside a baffled agitated vessel mounted with a 6 blade PBT impeller using CFD analysis. The analysis of flow field results in the calculation of instantaneous velocity, with the long-term averaged mean velocity and also the random component that is useful to determine the energy dissipation pattern in the vessel along with the structure and decay of turbulence, (Mavros, P. et al, 1998).

6.2 Numerical Computation of Flow Field

In the present work, flow field inside a vessel was analyzed numerically to ascertain uniform axial flow pattern in the tank. The transient simulations were performed in ANSYS Fluent for five different rotational speeds of the impeller ranging between 100-900 rpm. The run-time for transient analysis was selected on the basis of the mixing time, t_m (described in Chapter III) for different Reynolds numbers corresponding to rotational speeds. The run-time chosen on the basis of mixing time for five different rotational speeds is tabulated in Table 6.1.

Table 6.1: Run-time for simulations based on mixing time

Rotational Speed, n (rpm)	**Simulation run-time (s)**
100	30
300	10
500	5
700	5
900	4

The following section describes the solution procedure adopted to numerically analyze the flow field in the vessel along with boundary conditions.

6.3 Solution Procedure

CFD simulations on the discretized model of agitated vessel were performed in ANSYS Fluent. As the number of mesh elements generated was more than 2 million, to save computation time, parallel processing was utilized to perform simulations using multiple processors. The facility for computation was provided by Czech Technical University's computation servers. The journal files containing all the necessary commands for execution by the solver of ANSYS Fluent (in batch mode) were created for different rotational speeds.

The journal file written for rotational speed of 100 rpm and simulation run time of 30 seconds is shown below:

```
; fluent150t 3ddp -t 16 -g -i fluent.in
/file/read-case-data init.cas.gz
;
; will overwrite files without a confirmation
/file/confirm-overwrite no
;
; rotation speed definition
/define/parameters/input-parameters   edit   "rotation-speed"   "rotation-
speed" 100
;
; first - switch energy off and perform some steady-state iterations
/define/models energy no
/define/models steady yes

/solve/iterate 2000
; save steady-state
/file/write-case-data steady.cas.gz
;
; switch to transient model
/define/models unsteady-1st-order yes
; switch energy on + dissipation: no, pressure work: no, kinetic energy:
no,
;   diffusion at inlets: yes
/define/models energy yes no no no yes
;
/solve/set time-step 0.001
;/solve/set max-iterations-per-time-step 20
;/solve/set data-sampling yes 1 yes yes yes
/solve/set extrapolate-vars yes
; init statistics
/solve/init/init-flow-statistics
;
/define/parameters/output-parameters/print-all-to-console
/define/parameters/output-parameters/write-all-to-file params0.out
;
; perform first set of iterations

/solve/dual-time-iterate 30000 20
;
; define mean heat transfer coefficients, they are not defined before
some statistics is collected
```

```
/define/parameters/output-parameters/create/surface-integral  "mean-alpha"
area-weighted-avg mean-heat-transfer-coef tank-bottom tank-wall ()
/define/parameters/output-parameters/create/surface-integral  "mean-alpha-
bottom" area-weighted-avg mean-heat-transfer-coef tank-bottom ()
/define/parameters/output-parameters/create/surface-integral  "mean-alpha-
wall" area-weighted-avg mean-heat-transfer-coef tank-wall ()
;
; print all parameters to console
/define/parameters/output-parameters/print-all-to-console
/define/parameters/output-parameters/write-all-to-file params1.out
/file/write-case-data trans1-%t.cas.gz
;
; init statistics for the next set of time steps
/solve/init/init-flow-statistics
; perform another set of iterations/time steps

/solve/dual-time-iterate 30000 20
/define/parameters/output-parameters/print-all-to-console
/define/parameters/output-parameters/write-all-to-file params2.out
/file/write-case-data trans2-%t.cas.gz
;
/exit yes
```

Similar journal files as described above were written for the impeller rotation speeds of 300-900 rpm. The ANSYS Fluent (in batch mode) sequentially executes the commands written in the journal files. The semi-colon operator ';' in the script before the start of a line indicates that the commands or statements will not be executed and treats it as a comment. The output results were stored as separate files with an extension '.out'.

The following sub-sections describe the solution strategy utilized in ANSYS Fluent.

6.3.1 Material

The chosen material (the working fluid) in the agitated vessel was 'water' with constant thermo-physical properties at 25^{o}C.

6.3.2 Solver

Pressure based solver was selected for the simulations. The first 2000 iterations were performed for steady-state case (to attain a fully-developed flow profile in the tank) and after that the calculations were switched to transient model. The time step chosen for transient analysis was 0.001 s.

The time step was estimated on the basis of an average cell size and tip velocity of the impeller as:

$$\Delta t = \frac{\Delta x}{u_{tip}} \tag{6.1}$$

where Δt is the estimated time step, Δx is the average cell size and u_{tip} is the tip velocity of the impeller. The tip velocity can be obtained as:

$$u_{tip} = \omega_i R \tag{6.2}$$

where ω_i is the angular velocity and R is the radius of the impeller. The maximum iterations per time step were 20 for all the simulations. The run-time for transient analysis was selected on the basis of the mixing time, t_m for different rotational speeds.

6.3.3 Cell Zone Conditions

The simulations were performed using Sliding Mesh technique available in ANSYS Fluent. The impeller region was given a rotation with specific rotation speed while the region outside the impeller was kept stationary.

6.3.4 Boundary Conditions

The wall motion for the impeller (including shaft) was set as 'moving wall'. The motion was kept absolute with a rotational component. The 'no slip' was applied as shear condition. The baffles and tank walls were set as stationary walls.

6.3.5 Solution Method

The $k - \omega$ based Shear-Stress-Transport (SST) turbulence model (described in Chapter IV) was chosen to model turbulence. The SIMPLE algorithm was chosen for Pressure-Velocity coupling. The second-order accurate upwind scheme for momentum, turbulent kinetic energy, specific dissipation rate and energy was selected. The upwind scheme in ANSYS Fluent is used for the interpolation of face values (required for the convection terms in the discretized scalar transport equation) from the stored cell-center values of the field variables. Standard initialization was performed and the calculations were run till the residuals of continuity and components of velocity were less that 1e-03. For temperature, 1e-06 was used.

6.4 Computational Results

The post-processing results in ANSYS CFD-Post for transient simulations at N = 500 rpm and corresponding Reynolds number of 36860 are described in the following sub-sections:

6.4.1 The velocity field

The axial flow pattern was developed by the PBT impeller rotating inside the agitated vessel. The velocity vector plot for the obtained flow pattern is shown in Figure 6.1 and the velocity contour plot is shown in Figure 6.2.

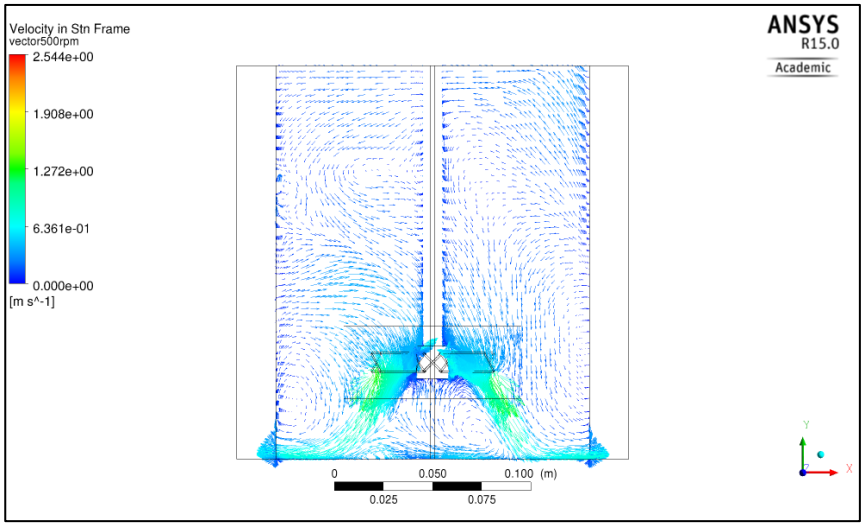

Fig. 6.1: Axial flow pattern generated by the PBT impeller discharging the flow downward towards vessel bottom

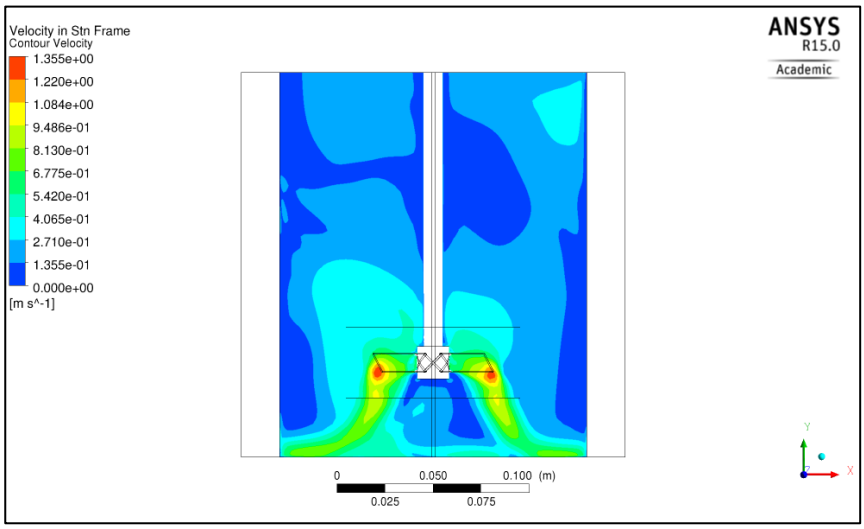

Fig. 6.2: Velocity contour plot for Re = 36860

The normalized axial velocity profile in terms of non-dimensional velocity, u_y/u_{tip} and non-dimensional radius, r/R obtained by defining a horizontal line at a height Z/T = 0.016 m (just below the impeller blades) for Re = 36860 is shown in Figure 6.3. The u_y represents the axial components of the instantaneous velocities, u_{tip} is the tip velocity of the impeller, R is the radius of impeller and r is the radial distance.

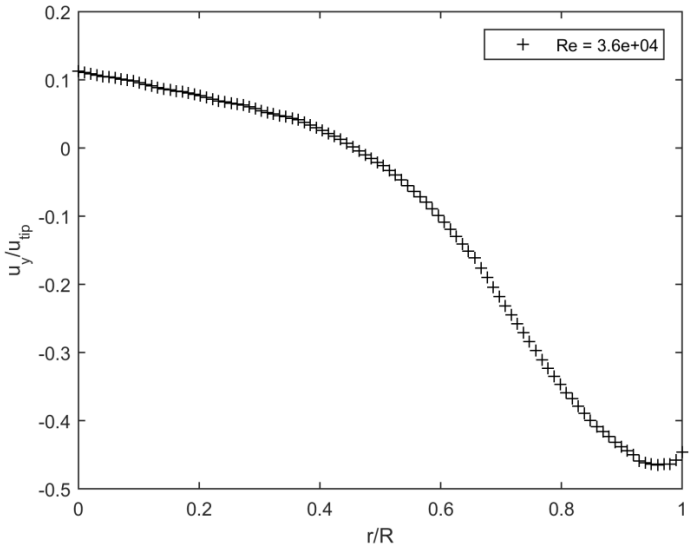

Fig. 6.3: Axial velocity profile in the discharge flow of the PBT impeller

It can be observed from the axial velocity profile that the discharge from the impeller is downward and the velocity gradient is rather steep as it approaches the boundary region surrounding the impeller.

6.4.2 Checking y^+ at the tank surfaces

To resolve the near-wall regions where the occurrence of momentum and other scalar transports is relatively high, wall functions are usually needed with the disadvantage of an increase in computational error. In the present work, to avoid using wall functions in treating near-wall regions, an attempt was made to reach the recommended y^+ value equal to 1. During the computational grid generation, the inflation layers were applied to capture the near-wall gradients more accurately. The y^+ was checked after performing the simulations and the obtained values of y^+ for the tank bottom, tank walls and the baffles were found to be within the acceptable range and hence no wall functions were applied. The obtained y^+ for the tank bottom, tank walls and the baffles are shown in Figure 6.4, 6.5 and 6.6 respectively.

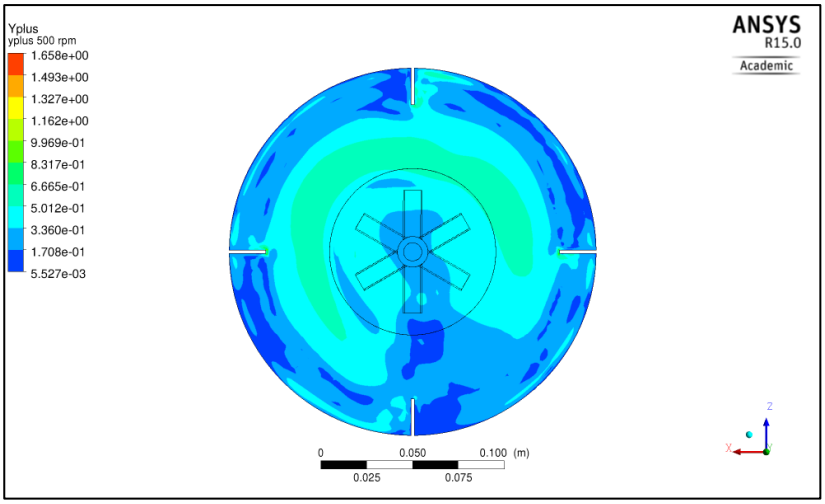

Fig. 6.4: y^+ range for the tank bottom at $n = 500$ rpm

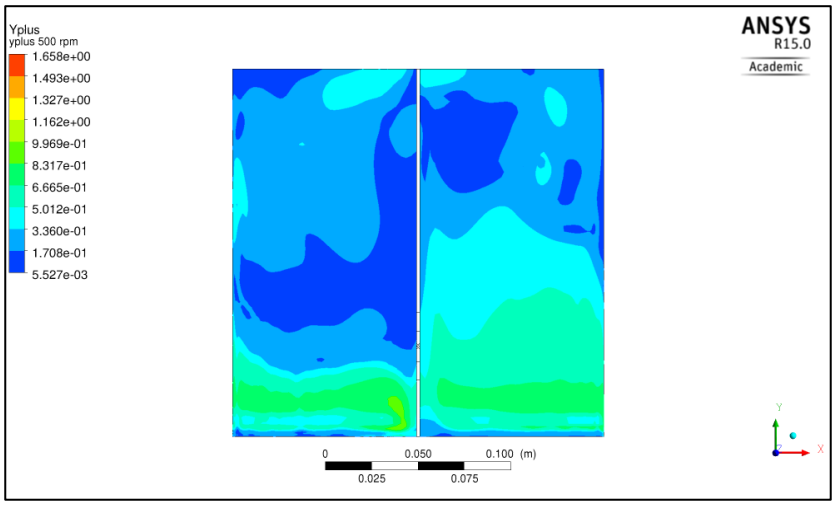

Fig. 6.5: y^+ range for the tank wall at $n = 500$ rpm

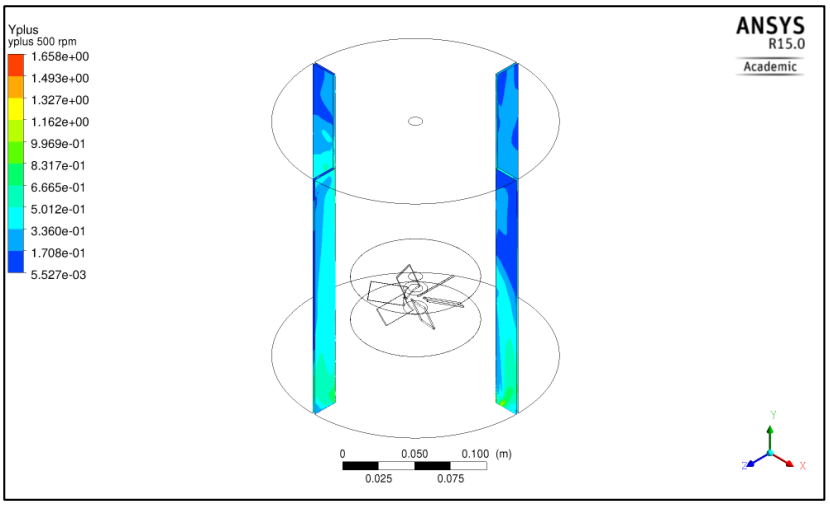

Fig. 6.6: y^+ range for the tank baffles at $n = 500$ rpm

Chapter VII Examination of Spatial (Grid) Convergence

7.1 Introduction

The evaluation of spatial (grid) convergence is a method to determine ordered discretization error in a CFD simulation. The method requires simulations to be performed on two or more successively finer grids. The refinement of the grid results in an increase in the number of mesh elements and a decrease in the cell size present in the flow domain. The refinement can be spatial and/or temporal. The temporal refinement deals with the reduction in the size of time step. As the grid is refined, the spatial and temporal discretization errors should asymptotically approach zero, excluding the round-off errors.

7.2 Method – Grid Convergence Index

A method developed by Roache, (1998) and based on Richardson extrapolation suitable for analyzing the grid convergence is determining the Grid Convergence Index (GCI) value for the different levels of grids. The minimum number of levels of grid to evaluate GCI is two. However, three levels of grid are usually recommended in order to accurately estimate the order of convergence and to check whether the solutions are within asymptotic range of convergence. The GCI value for a particular grid level indicates the inaccuracy in the obtained solution from that of exact solution.

7.3 Evaluation of Grid Convergence Index

The dependency of solution on the number of mesh (grid) cells (or elements) can be described by the following relation:

$$\Phi = \Phi_{\text{ext}} + aN^{-p/L} \tag{7.1}$$

where Φ_{ext} represents the extrapolated value of the solution for infinitely large mesh size, a represents a model parameter, N represents the number of mesh elements, p is the order of convergence representing the solution accuracy, L equals 2 for 2D mesh and 3 for 3D mesh.

The three unknown parameters Φ_{ext}, a and p can be calculated from three equations for three different mesh sizes as:

$$\Phi_1 - \Phi_{\text{ext}} - aN_1^{\,-p/L} = 0 \tag{7.2}$$

$$\Phi_2 - \Phi_{\text{ext}} - aN_2^{\,-p/L} = 0 \tag{7.3}$$

$$\Phi_3 - \Phi_{\text{ext}} - aN_3^{\,-p/L} = 0 \tag{7.4}$$

In terms of the average (characteristic) size of mesh elements, h where h equals the reciprocal value of the number of mesh elements, N. The Eq. (7.1) can be written showing dependency of solution on element size as:

$$\Phi = \Phi_{\text{ext}} + ah^p \tag{7.5}$$

where h is the characteristic mesh size given by $h = -(1/N)^{\frac{1}{L}}$ or $h = -(V/N)^{\frac{1}{L}}$ where V is the volume of cell. It can be observed from Eq. (7.5), as the element size is decreased by increasing the number of mesh elements, N the solution approaches the extrapolated solution and for a theoretical case of $h = 0$, i.e $N \to \infty$, the solution is the accurate solution equal to Φ_{ext} .

The three equations in terms of three different characteristic mesh sizes can be written as:

$$\Phi_1 - \Phi_{\text{ext}} - ah_1^{\,p} = 0 \tag{7.6}$$

$$\Phi_2 - \Phi_{\text{ext}} - ah_2^{\,p} = 0 \tag{7.7}$$

$$\Phi_3 - \Phi_{\text{ext}} - ah_3^{\,p} = 0 \tag{7.8}$$

Subtracting Eq. (7.7) from (7.6), we obtain:

$$\Phi_1 - \Phi_2 = ah_1^{\,p}\left[1 - \left(\frac{h_2}{h_1}\right)^p\right] = ah_1^{\,p}\left(1 - r_{21}^p\right) \tag{7.9}$$

where $r_{21}^p = h_2/h_1$ is refinement ratio for finest grid size. Similarly, subtracting Eq. (7.8) from (7.7), we obtain:

$$\Phi_2 - \Phi_3 = ah_2^{\,p}\left[1 - \left(\frac{h_3}{h_2}\right)^p\right] = ah_2^{\,p}\left(1 - r_{32}^p\right) \tag{7.10}$$

where $r_{32}^{p} = {}^{h_3}/_{h_2}$ is refinement ratio for mid-size grid level. Dividing the Eq. (7.9) and Eq. (7.10) yields:

$$\frac{\Phi_1 - \Phi_2}{\Phi_2 - \Phi_3} = \frac{1}{r_{21}^{p}} \frac{1 - r_{21}^{p}}{1 - r_{32}^{p}} \tag{7.11}$$

The differences between particular variables can be written as:

$\varepsilon_{21} = \Phi_2 - \Phi_1$ and $\varepsilon_{32} = \Phi_3 - \Phi_2$

and Eq. (7.11) can be rearranged in the form:

$$r_{21}^{p} \frac{\varepsilon_{21}}{\varepsilon_{32}} = \frac{r_{21}^{p} - 1}{r_{32}^{p} - 1} \tag{7.12}$$

Applying logarithmic function , we obtain:

$$lnr_{21}^{p} + ln\frac{\varepsilon_{21}}{\varepsilon_{32}} = ln\frac{r_{21}^{p} - 1}{r_{32}^{p} - 1} \tag{7.13}$$

and separating p from first term of Eq. (7.13), the order of convergence, p can be described as:

$$p = \frac{1}{lnr_{21}} \left[ln\frac{\varepsilon_{32}}{\varepsilon_{21}} + ln\frac{r_{21}^{p} - 1}{r_{32}^{p} - 1} \right] \tag{7.14}$$

This relation is similar to the equation published by Celik (2008):

$$p = \frac{1}{lnr_{21}} \left| ln\left| {}^{\varepsilon_{32}}/_{\varepsilon_{21}} \right| + q \right|, \qquad q = ln\left(\frac{r_{21}^{p} - s}{r_{32}^{p} - s} \right), \quad s = sign\frac{\varepsilon_{32}}{\varepsilon_{21}} \tag{7.15}$$

The absolute values and the sign function in Eq. (7.15) are for situations in which there is non-monotonous increase or decrease of the monitored quantity (For e.g. $\Phi_1 < \Phi_2$ and $\Phi_2 > \Phi_3$). The equation for p is solved numerically.

The parameter, a from Eq. (7.6) can be expressed as:

$$a = \frac{\Phi_1 - \Phi_{\text{ext}}}{{h_1}^p} \tag{7.16}$$

and substituting the expression of a in Eq. (7.7),

$$\Phi_{\text{ext}} = \frac{\Phi_1 r_{21}^p - \Phi_2}{r_{21}^p - 1} \tag{7.17}$$

and the accuracy of Φ_1 solution for the finest mesh in terms of GCI is:

$$GCI_{21} = F_s \frac{\Phi_{\text{ext}} - \Phi_1}{\Phi_1} \tag{7.18}$$

where F_s is the factor of safety in the estimation of numerical accuracy. Substituting Φ_{ext} in Eq.(7.18) with F_s of 1.25 , we obtain fine-grid convergence index:

$$GCI_{21} = \frac{1.25 e_a^{21}}{r_{21}^p - 1} \tag{7.19}$$

where e_a^{21} is the approximate relative error,

$$e_a^{21} = \left|\frac{\Phi_1 - \Phi_2}{\Phi_1}\right| \times 100\ [\%] \tag{7.20}$$

Similar relation for GCI of mid-size mesh can be written as:

$$GCI_{32} = \frac{1.25 e_a^{32}}{r_{32}^p - 1} \tag{7.21}$$

It is recommended that the refinement ratios, r_{21}^p and r_{32}^p be greater than 1.3, (Celik, 2008).

7.4 Calculation of Grid Convergence Index

In the present work, the GCI was evaluated to determine the appropriate mesh size for conducting unsteady heat transfer analysis with reasonable accuracy. The model of the agitated vessel was discretized into three different mesh sizes. The three successive finer mesh sizes had 1080381, 2269507 and 4564764 elements respectively.

The simulations were performed in ANSYS Fluent for a rotation speed of 500 rpm. The MRF (Moving Reference Frame) approach was chosen to model the flow around the impeller. The torque, M_t values were monitored and the average values were used to evaluate the GCI_{21} and GCI_{32} for the finest mesh and mid-size mesh respectively. The order of convergence, p was calculated numerically by solving Eq. (7.15) using '*fsolve'* procedure of MATLAB.

The calculated GCI values with numerical accuracy parameters are tabulated in Table 7.1.

Table 7.1: Calculation of discretization error

	$\Phi = M_t$ at 500 rpm (non-monotonic dependency)
N_1, N_2, N_3	4564764, 2269507, 1080381
r_{21}	1.26
r_{32}	1.28
Φ_1	2.4587476737e-02
Φ_2	2.4640680896e-02
Φ_3	2.4570484468e-02
p	1.1492
${\Phi_{ext}}^{21}$	0.0244
${e_a}^{21}$	0.21 %
${GCI_{fine}}^{21}$	0.88 %
${e_a}^{32}$	0.28 %
${GCI_{mid-size}}^{32}$	1.08 %

The numerical uncertainty in the fine-grid solution was found to be 0.88 % and for the mid-size grid solution 1.08 %. It is to be noted that the numerical uncertainty predicted by the GCI values does not account for the modeling and computational round-off errors.

The GCI values are very good, the coarsest mesh with 1 million mesh elements could also give results with satisfying accuracy. But we decided to use the mid-size mesh in order to get values of Y+ around 1 at the vessel wall (which is crucial for good prediction of heat transfer) which could not be achieved by the coarsest mesh.

The MATLAB code for estimating GCI_{fine}^{21} and $GCI_{mid-size}^{32}$ is described below:

```
N = [4564764 2269507 1080381];
Phi = [ 2.4587476737e-02 2.4640680896e-02 2.4570484468e-02 ];

figure(1);
plot(N,Phi,'r*', N,Phi,'b');
grid on;

L = 3; % dimension of the problem, 2-D or 3-D

r21 = (N(1)/N(2))^(1/L)
r32 = (N(2)/N(3))^(1/L)
if ( r21 < 1.3 || r32 < 1.3 )
  disp('refinement factors r21 and r32 should be greater than 1.3');
end

eps32 = Phi(3)-Phi(2)
eps21 = Phi(2)-Phi(1)
R = eps21/eps32
s = sign(eps32/eps21)

fq = @(p) log((r21.^p-s)./(r32.^p-s));
fp = @(p) p - 1/log(r21)*abs(log(abs(eps32/eps21))+fq(p));
p = fsolve(fp,1) % numerical procedure to calculate p

Phi21ext = (r21^p*Phi(1)-Phi(2))/(r21^p-1)
e21a = abs((Phi(1)-Phi(2))/Phi(1))*100
GCI21 = 1.25*e21a/(r21^p-1)% uncertainty in fine-grid solution
e32a = abs((Phi(2)-Phi(3))/Phi(2))*100
GCI32 = 1.25*e32a/(r32^p-1)% uncertainty in mid-size grid solution
```

The observed dependency of monitored quantity was found to be non-monotonous (shown in Figure 7.1) which causes oscillatory convergence (with decreasing amplitude).

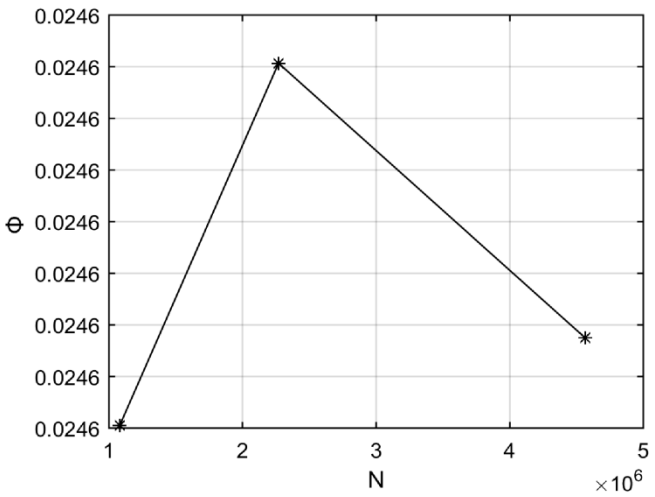

Fig. 7.1: Non-monotonic dependency of the monitored quantity

Chapter VIII Power Characteristics of Impeller

8.1 Introduction

In industrial mixing applications, the design of a mixing vessel depends on the input power required by the electric motor to drive the impeller rotating inside the vessel filled with process fluid. It is necessary to determine power characteristics of an impeller to know the amount of power required by the impeller (with specific geometrical parameters and type) operating at a given rotational speed.

8.2 Dimensionless Group – Power number

It has been experimentally found by researchers that the power P of a given impeller type and for particular mounting conditions (vessel diameter T, liquid height H, impeller bottom clearance C) in a homogeneous fluid depends on the impeller diameter d, the presence of baffling, the fluid parameters (like dynamic viscosity μ and density ρ) and impeller speed,n. The above mentioned dependence on dimensional parameters can be expressed as:

$$f_1(P, d, T, H, C; \mu, \rho; n) = 0 \tag{8.1}$$

The application of dimensionless analysis to the dependence shown in Eq. (8.1) was investigated by Rushton et al. (1950) and they described a reduced dependence in terms of dimensionless groups as:

$$f_2(Po, Re, T/d, H/d, C/d) = 0 \tag{8.2}$$

where Po is called Power number (or sometimes called Newton number) and Re is the Reynolds number. The Power number Po is expressed as:

$$Po = \frac{P}{\rho n^3 d^5} \tag{8.3}$$

The dependence (8.2) is called the power characteristic of an impeller.

8.3 Calculation of Power number for 6 Blade PBT Impeller

In the present work, the input power required for the 6 blade PBT impeller was measured for five different rotational speeds ranging between 100-900 rpm. The torque was measured numerically as a monitored quantity in ANSYS Fluent. The power required was calculated as the average torque multiplied by the angular velocity of the impeller. The Power number Po was then evaluated using Eq. (8.3). The results for Power number are tabulated in Table 8.1.

Table 8.1: Calculation of Power number

Rotational speed, n (rpm)	**Re [-]**	**Po [-]**
100	7372	1.66
300	22116	1.72
500	36860	1.77
700	51604	1.81
900	66348	1.82

The functional relationship of $Po(Re)$ was plotted and is shown in Figure 8.1.

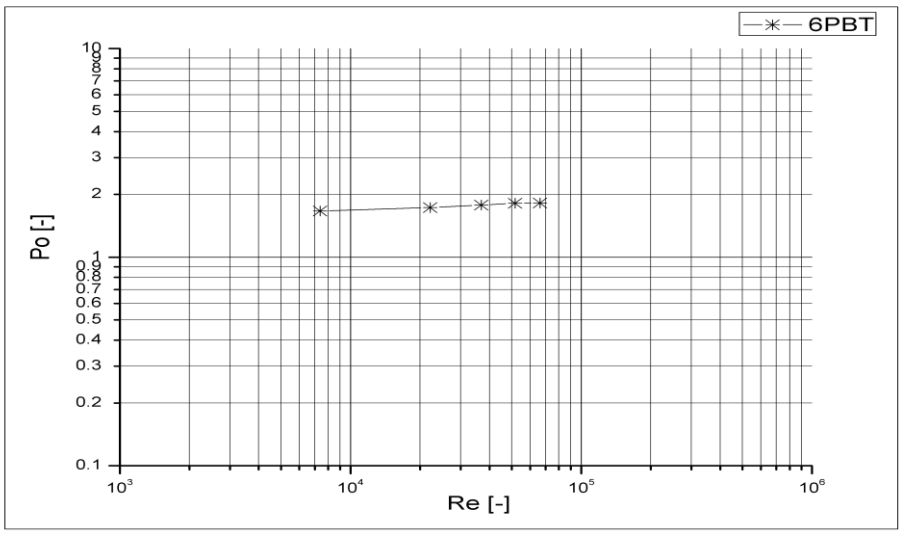

Fig. 8.1: Obtained power characteristic of 6 blade PBT impeller in turbulent flow regime

It can be observed from the power characteristic of the PBT impeller (Figure 8.1) that the Power number Po approaches a constant value with an increasing Reynolds number Re, which is experimentally proven for a mixing process occurring in turbulent flow regime.

To check whether the description of the Power number by a constant value was statistically accurate, the F-test was performed to compare the power model and the null hypothesis. The power model can describe the non-linear relationship between the Reynolds number and Power number as:

$$Po = a\, Re^{b} \tag{8.4}$$

where a and b in Eq. (8.4) are the model parameters. The null hypothesis is a simpler model compared to power model. The goal of F-test was to ascertain whether only a constant value of Power number is sufficient (described by null hypothesis) or the power model gives more accurate description of the functional relationship between the Power number and the Reynolds number. The non-linear regression was performed in MATLAB using the '*nlinfit*' procedure. The 'nlinfit2' function file was written and was utilized to perform the F-test to determine whether there is a significant difference between the two models. The 'nlinfit2' function file written in MATLAB (compatible with OCTAVE) is shown below:

```
function [ a, resid, Jc, ci, cip, cipp ] = nlinfit2(Xi,Yi,fmodel,Binit)
np = length(Binit);

if  (~ exist('OCTAVE_VERSION'))
  [a,resid,Jc,covb] = nlinfit(Xi,Yi,fmodel,Binit);
  ci = nlparci(a,resid,'jacobian',Jc,'alpha',1-0.95);
  cip = a' - ci(:,1);
else
  % leasqr in Octave expects opposite order of input parameters
  fmodel2 = @(x,a) fmodel(a,x);
  [y2,a,kvg,iter,corp,covp,covr,stdresid,Z,r2]                              =
leasqr(Xi,Yi,Binit,fmodel2);
  %%beta = a;
  resid = Yi - y2; % residua
  N = length(Xi);
  nf = N-np;
  Sv2 = sum(resid.^2)/nf;
  %covp
  Jc = [];
  C = sum(stdresid.^2)/nf*covp;
  t975 = tinv(0.975,nf);
  for i=1:np;
    stde(i) = sqrt(C(i,i));
    cip(i) = stde(i)*t975;
    ci(i,:) = [a(i)-cip(i),a(i)+cip(i)];
  end
end

cipp = cip./abs(a')*100;
for i=1:np;
  fprintf('beta(%d):    %12f    +-    %10f    (%.2f%%),           %12f    ...
%12f\n',i,a(i),cip(i),cipp(i),ci(i,:));
end
```

The MATLAB script written for performing non-linear regression and the F-test using the 'nlinfit2' function is shown below:

```
format compact;
data = xlsread('power2.xlsx');

Xi = data(:,1);
Yi = data(:,2);

fmodel = @(b,x) b(1)*x.^b(2); %power model
[b,resid,J] = nlinfit2(Xi,Yi,fmodel,[1 1]);
b
SSalt = sum( resid.^2 )
N = length(Xi)
DFalt = N - 2

fmodel1 = @(b,x) b(1)*x.^0; %null hypothesis
[b0,resid0,J0] = nlinfit2(Xi,Yi,fmodel1,[1]);
b0
SSnull = sum( resid0.^2 )
DFnull = N - 1
F = ( (SSnull-SSalt)/SSalt )/( (DFnull-DFalt)/DFalt )
Fcrit = finv(0.95,DFnull-DFalt,DFalt)

Pr = fcdf(F,DFnull-DFalt,DFalt)
p = 1-Pr

if ( F < Fcrit )
    disp('no significant difference');
else
    disp('significant difference');
end

y1 = fmodel(b,Xi);
y0 = fmodel1(b0,Xi);
loglog(Xi,Yi,'r*', Xi,y1, Xi,y0);
```

The best fit parameters of the non-linear regression describing the two regression models of null hypothesis (constant value) and power model were obtained. It was found that the Power number predicted by the null-hypothesis was 1.76 ± 0.08 (4.56%) which was compared with the average value obtained in an experimental work performed by Beshay K.R et.al. (2001). For similar tank geometrical parameters ${}^{C}/_{T} = 0.2$, ${}^{H}/_{T} = 1$ and similar 6 blade PBT impeller with blade angle 45^{o}, they obtained an average power number of 1.84 which fits in the confidence interval of the Power number evaluated from the simulations in this work.

However, by performing F - test, it was found that there was a significant difference between the null hypothesis and the power model. The obtained best fit parameters of the power model described by Eq. (8.4) were $a = 1.13 \pm 0.13$ (11.45%) and $b = 0.042 \pm 0.011$ (26.06%). Due to the significance obtained in F - test, it is suggested to use the power model to describe the functional relationship between the Power number and the Reynolds number rather than describing the Power number with a constant value.

The log-log plot showing the non-linear fit for the power model and the constant value obtained by null hypothesis is shown in Figure 8.2.

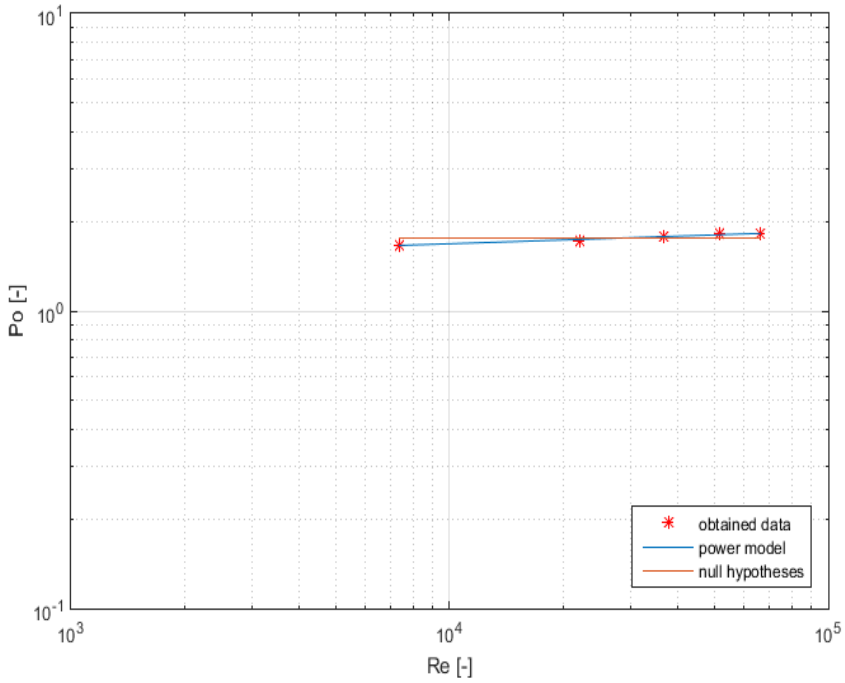

Fig. 8.2: Functional relationship between Power number Po and Reynolds number Re described by power model and null hypothesis

Chapter IX Transient Heat Transfer in Agitated Vessel

9.1 Introduction

The theory of heat transfer in agitated vessels was described in Chapter III. In process engineering applications involving heat transfer in agitated vessels, one of the vital information needed for the design and operation of the agitated vessel is the amount of heat transferred in a particular process (batch or continuous). The parameter that describes the amount of heat transferred is the overall heat transfer coefficient U that should be evaluated with reasonable accuracy for determining the size of the heat transfer surface needed to satisfy the heat duty requirements of the heat transfer process.

9.2 Transient (or unsteady) Heat Transfer

The time-dependent heat transfer is the so called transient heat transfer or unsteady heat transfer. In a jacketed agitated vessel, the steady state heat transfer is reached when the temperature of the jacket (or wall) and batch remains constant. This can be achieved only if a constant inlet (source) or outlet (sink) of heat is in balance with the heat removed through the vessel jacket.

The unsteady heat transfer occurs when the temperature of the batch changes during the agitation process from an initial temperature. The experimental readings of the batch temperature and jacket (or wall) temperature are usually taken versus time during the batch heating (or cooling). The advantage of transient analysis over steady state analysis is the fact that the time-dependence of heat transfer coefficients on the flow patterns affected by the presence of baffles and type of impeller can be studied whereas the disadvantage is the correction that must be applied for the changing fluid properties during heating (or cooling) of the batch.

9.3 Heat Transfer Surfaces

In practical situations involving heat transfer in an agitated vessel, it is often required to heat or cool a particular batch of process fluid while simultaneously agitating the batch. This heating or cooling can be intentional (to achieve final required product characteristics) or it can be a requirement (maintaining isothermal conditions due to the production of heat in a chemical reaction occurring inside the vessel). Therefore, the heating or cooling process in an agitated vessel depends on its particular industrial application.

However, one common thing that stays in both processes is the mechanism to dispose of the heat produced (cooling) or to transfer heat into the vessel (heating). The mechanisms employed to realize these heat transfer processes are the heat transfer surfaces that form an integral part of the vessel. One exception to this is the use of external heat exchangers for serving higher heat duties. The distinction between types of vessel on the basis of heat transfer surface was described in section 2.1.2, Chapter II. They can be classified as:

a) vessel with surrounding jacket
b) vessel with an internal heat transfer coil
c) vessel with external heat exchanger circuit

In the present work, the transient heat transfer was studied numerically in a cylindrical agitated vessel with a constant temperature heating medium at the wall. The assumption of constant temperature at tank walls simplified the calculations. In practical situations, the constant temperature of the wall can be assumed if the heating medium flowing in the vessel jacket is a condensing steam (or an evaporating liquid). However, this assumption is strongly affected by the mass flow rate of the heating medium.

9.4 Numerical Analysis of Heat Transfer

It was found by conducting a literature search in the field of heat transfer in agitated vessels that for agitated vessels mounted with PBT impeller, most of the numerical studies in the mixing technology so far are focused on studying the flow patterns, the mixing process itself and the power requirements during mixing with very little research devoted to the numerical analysis of heat transfer in vessels with PBT impeller. Therefore, one of the objectives of the present work was to analyze the numerical heat transfer in an agitated vessel with a PBT impeller.

9.5 Solution Procedure

The solution procedure in the ANSYS Fluent to analyze unsteady heat transfer was the same (section 6.3, Chapter VI) as for studying the flow field inside the agitated vessel. The transient heat transfer simulations were performed on the agitated vessel model (described in Chapter V) in the turbulent regime of flow using ANSYS Fluent for five different rotational speeds of the 6 blade PBT impeller ranging between 100-900 rpm. The energy equation was solved numerically to obtain the time-dependent temperature fields. The Sliding Mesh technique was used to model the flow around the impeller. The $k-\omega$ based SST turbulence model available in ANSYS Fluent was chosen to model turbulence. The time-dependence of temperature of the batch and process side heat transfer coefficients (monitored quantities) were evaluated for the bottom and wall surfaces of the agitated vessel while heating the batch with a constant temperature heating medium at wall. The wall temperature was set at 400 K.

9.6 Computational Results

The functional relationship between Nusselt number Nu and Reynolds number Re was determined to correlate the process side heat transfer coefficient h in terms of dependent variables.

9.6.1 Correction of ANSYS Fluent heat transfer coefficients

The differences between mean heat transfer coefficients reported by ANSYS Fluent and the heat transfer coefficients calculated by the heat balance were studied. The ANSYS Fluent evaluates the surface heat transfer coefficients h as:

$$h = \frac{q}{T_w - T_{ref}} \tag{9.1}$$

where q is the heat flux, T_w is the temperature of the vessel wall (constant in present study) and T_{ref} is the reference temperature which is used in ANSYS Fluent post-processing for the computation of derived quantities and non-dimensional coefficients. The reference temperature was set at 300 K as the initial temperature of the batch. Therefore, after the

simulations, the correction was applied to the obtained surface heat transfer coefficients. The correction was based on the calculated Logarithmic Mean Temperature Difference (LMTD).

The heat flux q from Eq. (9.1) was evaluated using the obtained surface heat transfer coefficients (named h - FLUENT).
The obtained surface heat transfer coefficients were recalculated by using LMTD as:

$$h - \text{FLUENT}_{corr} = \frac{q}{\Delta \bar{T}_{ln}} \tag{9.2}$$

where $h - \text{FLUENT}_{corr}$ is the corrected surface heat transfer coefficient and $\Delta \bar{T}_{ln}$ is the Log Mean Temperature Difference (LMTD) described as:

$$\Delta \bar{T}_{ln} = \frac{(T_w - T_{init}) - (T_w - T_{b2})}{ln\left(\frac{T_w - T_{init}}{T_w - T_{b2}}\right)} \tag{9.3}$$

where T_w is the wall temperature, T_{init} is the initial temperature (equal to T_{ref}) and T_{b2} is the final temperature of the batch. The evaluated heat transfer coefficients are tabulated in Table 9.1. The heat transfer coefficients obtained by means of ANSYS Fluent post-processing (Surface heat transfer coefficients) before applying correction are named h-FLUENT and those after correction are named $h - \text{FLUENT}_{corr}$. The heat transfer coefficients calculated from Eq. (3.9) are named h-CALC.

Table 9.1: Obtained heat transfer coefficients

Rotational speed, n (rpm)	**h-FLUENT** (W m^{-2} K^{-1})	**h-FLUENT$_{corr}$** (W m^{-2} K^{-1})	**h-CALC** (W m^{-2} K^{-1})	**Percentage difference** (%)	
				before correction	**after correction**
100	705.52	828.03	923.36	23.59	10.32
300	1735.19	1966.01	2147.15	19.18	8.43
500	2764.57	3039.24	3239.85	14.66	6.19
700	3673.86	4179.64	4438.31	17.22	5.82
900	4605.02	5245.13	5599.33	17.75	6.32

The effect of increasing impeller rotation speed on the obtained heat transfer coefficients is shown in Figure 9.1.

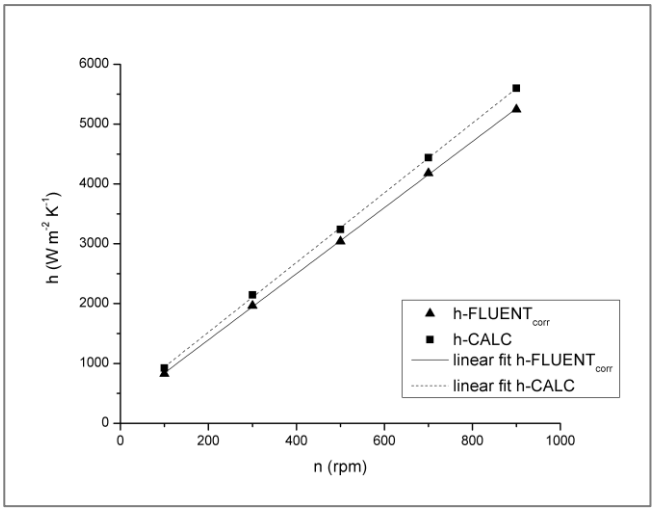

Fig. 9.1: Effect of varying agitation rate on the heat transfer coefficient

It can be observed from Figure 9.1 that the increase in agitation rate causes an increase in the heat transfer coefficient values. This is attributed to the increase in forced convection at higher rotational speeds.

9.6.2 Calculation of Nusselt number

For evaluating heat transfer to or from the vessel wall (or bottom) in a jacketed vessel the Nusselt number Nu is used which was described by Eq. (3.3) in Chapter III. The Nusselt numbers obtained from the simulation results were compared with the theoretical values for impeller rotation speeds ranging between 100-900 rpm. The obtained values of Nu are tabulated in table 9.2. The Nusselt numbers based on FLUENT post-processing of surface heat transfer coefficients are named Nu-FLUENT and those calculated according to heat balance Eq. (3.9) are named Nu-CALC.

Table 9.2: Obtained Nusselt numbers

Rotational speed, n (rpm)	**Nu-FLUENT** (-)	**Nu-CALC** (-)
100	276.01	307.78
300	655.33	715.71
500	1013.08	1079.95
700	1393.21	1479.43
900	1748.37	1866.44

9.6.3 Heat Transfer Correlation

The dependence of Nusselt number Nu on different variables is usually expressed as a combination of dimensionless groups in the form of heat transfer correlations. They were described in Chapter III. The general form of dependence of Nusselt number can be described as:

$$Nu = f(Re, Pr, geometrical\ parameters) \tag{9.4}$$

In general, the above dependence of Eq. (9.41) is presented by including the correction for temperature-dependent dynamic viscosity by including the Sieder-Tate correction similar as for forced convection in pipes. The correlation can be written as:

$$Nu = C\ Re^{a}\ Pr^{b} Vi^{c}\ G_{c} \tag{9.5}$$

where Vi is the Sieder-Tate correction with the exponent ' c' usually taken as 0.14 and $G_c$is the geometry correction factor. The other exponents of the correlation Eq. (9.5) are experimentally determined by performing regression analysis on the obtained experimental data.

In the present work, the heat transfer correlation for Nusselt number was found for a 6 blade PBT impeller for a constant Prandtl number Pr of 7.021. The temperature-dependence of thermo-physical properties of process fluid were neglected for simplicity. As the effect of variation of geometrical parameters such as the distance of the impeller from the bottom of the vessel C and varying impeller diameters D was not studied in this work, the geometry correction factor G_c was taken unity.

Two correlations were developed by performing one-parameter non-linear regression in MATLAB describing the dependence of Nusselt number (obtained by post-processing of surface heat transfer coefficients in ANSYS Fluent) on Reynolds number and the dependence of Nusselt number (obtained by calculating heat balance) on the Reynolds number for a 6 blade PBT impeller.

The values of Nusselt number with corresponding Reynolds number are tabulated in Table 9.3.

Table 9.3: Calculated Nu for different Re

Re (-)	Nu-FLUENT (-)	Nu-CALC (-)
7372	276.01	307.78
22116	655.33	715.71
36860	1013.08	1079.95
51604	1393.21	1479.43
66348	1748.37	1866.44

The one-parameter non-linear regression was performed using '*nlinfit*' procedure of MATLAB. The exponent 'a' of Re in Eq. (9.5) was fixed as the commonly used value of 0.66 and exponent 'b' of Pr was kept as 0.33. The regression paramenter 'C' in Eq. (9.5) was evaluated. The MATLAB code (compatible with OCTAVE) that was written defining the function '*nlinfit2*' was described in Chapter VIII for calculating the regression parameters with the confidence intervals. The MATLAB script written to calculate regression parameter with the confidence interval for Nusselt number data computed by CFD analysis using the '*nlinfit2*' is:

```
data = load('datafluent.txt');
size(data)
Xi = data(:,1);
Yi = data(:,2);
Pr = 7.021;
fmodel = @(b,x) b(1)*x.^(2/3)*Pr^(1/3);
[b,resid,J] = nlinfit2(Xi,Yi,fmodel,[1]);
x = linspace(min(Xi),max(Xi),30);
y = fmodel(b,x);
loglog(Xi,Yi,'r*', x,y,'b-');
```

and the MATLAB script to calculate regression parameter with the confidence interval for Nusselt number data computed from heat balance using '*nlinfit2*' is :

```
data = load('datacalculated.txt');
size(data)
Xi = data(:,1);
Yi = data(:,2);
Pr = 7.021;
fmodel = @(b,x) b(1)*x.^(2/3)*Pr^(1/3);
[b,resid,J] = nlinfit2(Xi,Yi,fmodel,[1]);
x = linspace(min(Xi),max(Xi),30);
y = fmodel(b,x);
loglog(Xi,Yi,'r*', x,y,'b-');
```

where ‘datafluent.txt’ and ‘dataclaculated.txt’ were written as the text files containing data for non-linear one-parameter regression analysis.

For constant exponents of Re as 2/3 and Pr as 1/3 in Eq. (9.5), by non-linear regression analysis, C (for Nusselt numbers based on ANSYS Fluent post-processing of surface heat transfer coefficients) was found to be equal to 0.517 $\pm$ 0.062 (12.02 %) and C (for the Nusselt numbers calculated by the heat balance) was found to be equal to 0.552 $\pm$ 0.062 (11.26 %).

The two heat transfer correlations developed in this work can be described as:

$$Nu = 0.517\, Re^{2/3}\, Pr^{1/3} \tag{9.6}$$

and

$$Nu = 0.552\, Re^{2/3}\, Pr^{1/3} \tag{9.7}$$

where Eq. (9.6) represents the process-side heat transfer correlation obtained by the ANSYS Fluent evaluation of unsteady heat transfer in a cylindrical agitated vessel mounted with a 6 blade PBT impeller and Eq. (9.7) represents process-side heat transfer correlation obtained on the basis of heat balance calculations.

The obtained heat transfer correlations are valid for a fluid of constant Prandtl number equal to 7.021 and for Reynolds number range $7 \times 10^4 < Re < 7 \times 10^5$. The above obtained correlations were compared to the experimentally obtained heat transfer correlations for PBT impellers in baffled vessels developed by Chapman et al. (1964) and described by:

$$Nu = 0.74\, Re^{2/3}\, Pr^{1/3}\, Vi^{0.14} \left(\frac{S_{bl}/D_i}{1/5} \right)^{0.2} \left(\frac{N_{bl}}{6} \right)^{0.2} [sin(\theta)]^{0.5} \tag{9.8}$$

where S_{bl} is the width of blade, D_i is impeller diameter, $N_{bl}$is number of blades and θ is pitch angle of blade. They performed experiments in the turbulent regime with Reynolds number reaching 10^5. For our geometrical specifications, i.e. S_{bl} = 0.0133 m , N_{bl} = 6 and θ = 45^o, the leading factor 0.74 in Eq. (9.8) changes to 0.62 which was close compared to the correlations obtained in this work, Eq. (9.6) and Eq. (9.7).

The obtained heat transfer correlations were compared with the experimental work of Chapman et al. (1964), Eq. (9.8) and the log-log plot showing the fitted correlations with their comparison with the experimental work are shown in Figure 9.2. It is observed a good agreement with the experimental work.

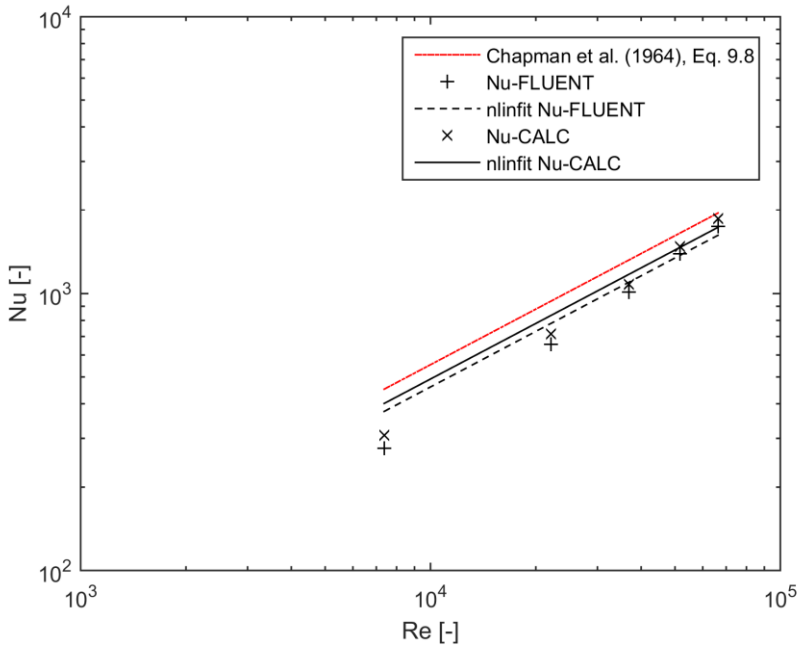

Fig. 9.2: Obtained data and fitted correlations compared with the experimental work of Chapman et al. (1964)

The validity of the obtained correlations in this work may be confirmed by conducting experimental studies involving agitated vessel equipped with a 6 blade PBT impeller. The heat transfer correlations can be used to calculate the process side heat transfer coefficients in the Reynolds number range $7 \times 10^4 < Re < 7 \times 10^5$. After obtaining heat transfer coefficients, time required to heat the batch in an agitated vessel from an initial temperature can be calculated as:

$$\Delta t = \frac{m\, c_p}{U\, A} \ln\left(\frac{T_h - T_{b1}}{T_h - T_{b2}}\right) \tag{9.9}$$

where Δt is the time required to heat the batch in an agitated vessel from an initial temperature T_{b1} to final temperature T_{b2}. U is the overall heat transfer coefficient which is obtained as a sum of the resistances of heat flow from the jacket side to the process side including the conduction heat resistance of the vessel wall.

Conclusion and Further Scope

Concluding Remarks

The agitation process involving mixing with simultaneous heat transfer for a batch of fluid inside the agitated vessel is one of the most common process applications found in numerous process industries. The heat transfer correlations for given geometrical parameters of the vessel and impeller are used for estimating heat transfer coefficients needed to determine time required to heat or cool a batch inside the agitated vessel.

It was found that so far, a lot of research work has been devoted in studying the mixing process inside the agitated vessel with different types of impeller and vessel geometries but very few have focused on the analysis of the mixing process involving simultaneous heat transfer for a vessel equipped with a PBT impeller. Therefore, the present work was performed to analyze agitation process with simultaneous unsteady heat transfer in a baffled cylindrical agitated vessel mounted with a PBT impeller by using the CFD approach.

Summary of the main results

a. The literature search was done to find scientific works related to heat transfer in agitated vessels mounted with PBT impeller and it was observed that very few have been focused so far on the heat transfer analysis of the agitated vessel mounted with a PBT impeller.

b. The CFD analysis of agitated vessel with PBT impeller was performed:

i. The grid independency study was done to determine the acceptable mesh for the simulations.
ii. The solution strategy of the settings for the ANSYS Fluent solver was determined to perform transient simulations.
iii. The power characteristics of the PBT impeller was evaluated and compared with the experimental work of Beshay K.R et.al. (2001).

iv. The mean heat transfer coefficients were evaluated by performing simulations in ANSYS Fluent.

c. The heat transfer coefficients based on heat balance were also evaluated:

i. The correction of the heat transfer coefficients evaluated in ANSYS Fluent were performed so as to minimize large difference between the heat transfer coefficients based on heat balance and heat transfer coefficients obtained by simulations (as the ANSYS Fluent evaluates the heat transfer coefficients related to defined reference temperature).

ii. The functional relationship between Nusselt number and Reynolds number for a PBT impeller in a baffled vessel was studied by developing heat transfer correlations using non-linear regression analysis.

iii. The developed correlations were compared with the experimental work of Chapman et al. (1964) and a good agreement was obtained.

Further Scope related to the present work

The present work was aimed at analyzing the unsteady heat transfer in an agitated vessel mounted with a 6 blade PBT impeller using the CFD approach. However, experimental studies focused on estimating heat transfer in agitated vessels stirred with PBT impellers are needed to verify the validity of the CFD approach. Furthermore, in the present work, the spatial grid convergence was calculated based on the decrease in the size of grid. Another type of convergence that can be analyzed is the effect of reducing the time step (i.e. temporal convergence).

Some further works that can be studied related to the present work are:

a. The variation of geometrical parameters of the vessel and the impeller to determine the geometrical correction factor.

b. The effect of varying thermo-physical properties of the batch during heating/cooling.

c. The simulations based on other turbulence models like LES (Large eddy simulation), RSM (Reynolds stress model), etc.

References

1. ANSYS, Inc. (2006). *Fluent 6.3 User's Guide*, ANSYS, Inc.

2. Ascanio, G., Castro, B and Galindo, E. (2004). Measurement of power consumption in stirred vessels – a review, *Trans IChemE, Part A, Chem. Eng. Res. Des.*, v. 82 (A9), pp. 1282-1290.

3. Aubin, J., Fletcher, D.F and Xuereb, C. (2004). Modeling turbulent flow in stirred tanks with CFD: The influence of the modelling approach, turbulence model and numerical scheme. *Experimental, Thermal and Fluid Science*, v. 28, pp. 431-445.

4. Bakker, A., Myers, K.J., Ward, R.W and Lee, C.K. (1996). The laminar and turbulent flow pattern of a pitched blade turbine. *Trans IChemE*, v. 74, Part A, pp. 485-491.

5. Beshay, K.R., Kratěna, J., Fořt, I and Brůha, O. (2001). Power input of high-speed rotary impellers. *Acta Polytechnica*, v. 41(6), pp. 18-23.

6. Brodkey, R.S and Hershey H.C. (1988). *Transport Phenomena: a unified approach*, McGraw-Hill Book Co.

7. Celik, I.B., Ghia, U., Roache, P.J., Freitas, C.J., Coleman, H and Raad, P.E. (2008). Procedure for estimation and reporting of uncertainty due to discretization in CFD applications. *ASME J. Fluids Eng.*, v. 130 (7), pp. 078001-4.

8. Chapman, F.S., Dallenbach, H and Holland, F.A. (1964). Heat transfer in baffled, jacketed agitated vessels, *Trans. Inst. Chem. Engng.*, v. 42, pp. T398-T406.

9. Chapple, D., Kresta, S.M., Wall, A and Afacan, A., (2002).The effect of Impeller and tank geometry on power number for a pitched blade turbine. *Trans, IChemE*, v. 80, *Part A*, pp. 364-372.

10. Chisholm, D., ed. (1988). *Heat Exchanger Technology*, Elsevier Applied Science.

11. Dostál, M., Petera, K and Rieger, F. (2010). Measurement of heat transfer coefficients in an agitated vessel with tube baffles, *Acta Polytechnica*, v. 50 (2), pp. 46-57.

12. Dostál, M., Věříšová, M., Petera, K., Jirout, T and Fořt, I. (2014). Analysis of heat transfer in a vessel with helical pipe coil and multistage impeller, *Can. J. Chem. Eng.*, v. 92 (12), pp. 2115-2121.

13. Driss, Z., Bouzgarrou, G., Chtourou, W., Kchaou, H and Abid, M.S. (2010). Computational studies of the pitched blade turbines design effect on the stirred tank flow characteristics. *European Journal of Mechanics B/Fluids, Elsevier*, v. 29, pp. 236-245.

14. Guiraud, P., Costes, J and Bertrand, J. (1997). Local measurements of fluid and particle velocities in a stirred suspension. *Chemical Engineering Jourmal, Elsevier*, v. 68, pp. 75-86.

15. Marshall, E.M and Bakker, A. (2004). Computational fluid mixing, In Paul, E.L., Atiemo-Obeng, V.A. and Kresta, S.M. (Eds.). *Handbook of Industrial Mixing*, Hoboken, NJ: Wiley-Interscience, pp, 257-343.

16. Mavros, P., Xuereb, C and Bertrand, J. (1998). Determination of 3-D flow fields in agitated vessels by Laser Doppler Velocimetry: use and interpretation of rms velocities. *Trans, IChemE*, v.76, *Part A*, pp. 223-233.

17. Roache, P.J. (1998). Verifications of codes and calculations. *AIAA Journal*, vol. 36 (5), pp. 696-702.

18. Rushton, J.H., Costich, E.W and Everett, H. J., (1950). Power characteristics of mixing impellers, *Chem. Eng. Prog.*, v. 46(8), pp. 395-476.

19. Takeda, H., Narasaki, K., Kitajima, H., Sudoh, S., Onofusa, M and Iguchi, S. (1993). Numerical simulation of mixing flows in agitated vessels with impellers and baffles, *Computers Fluids*, v. 22 (2), pp. 223-228.

20. Tsui, Y.Y., Lin, S.C., Shen, S.J and Hu, Y.C. (2008). Analysis of the flow agitated by disc impellers with pitched blades. *Numerical Heat Transfer, Part A: Applications*, v. 53 (10), pp. 1091-1108.

21. Wichterle, K. (1994). Heat transfer in agitated vessels. *Chem.Eng.Sci*. v. 49 (9), pp. 1480-1483.

22. White, F.M. (1974). *Viscous Fluid Flow*, McGraw-Hill, Inc., New York.

23. Zlokarnik, M. (2001). *Stirring: Theory and Practice*, Wiley-VCH Verlag GmbH, Weinheim.